The Astronomical Journal, 131:1479–1500, 2006 March

A *SPITZER SPACE TELESCOPE* INFRARED SURVEY OF SUPERNOVA REMNANTS IN THE INNER GALAXY

William T. Reach, Jeonghee Rho, Achim Tappe, and Thomas G. Pannuti
Spitzer Science Infrared Center, California Institute of Technology, Pasadena, CA 91125; reach@ipac.caltech.edu

Crystal L. Brogan
Institute for Astronomy, University of Hawaii, 640 North A'ohoku Place, Hilo, HI 96720

Edward B. Churchwell, Marilyn R. Meade, and Brian Babler
Department of Astronomy, University of Wisconsin, 475 North Charter Street, Madison, WI 53706

Rémy Indebetouw
Astronomy Department, University of Virginia, Charlottesville, VA 22904

and

Barbara A. Whitney
Space Science Institute, 4750 Walnut Street, Boulder, CO 80303
Received 2005 August 24; accepted 2005 October 18

ABSTRACT

Using Infrared Array Camera (IRAC) images at 3.6, 4.5, 5.8, and 8 μm from the GLIMPSE Legacy science program on the *Spitzer Space Telescope*, we searched for infrared counterparts to the 95 known supernova remnants that are located within Galactic longitudes $65^\circ > |l| > 10^\circ$ and latitudes $|b| < 1^\circ$. Eighteen infrared counterparts were detected. Many other supernova remnants could have significant infrared emission but are in portions of the Milky Way too confused to allow the separation of bright H II regions and pervasive mid-infrared emission from atomic and molecular clouds along the line of sight. Infrared emission from supernova remnants originates from synchrotron emission, shock-heated dust, atomic fine-structure lines, and molecular lines. The detected remnants are G11.2−0.3, Kes 69, G22.7−0.2, 3C 391, W44, 3C 396, 3C 397, W49B, G54.4−0.3, Kes 17, Kes 20A, RCW 103, G344.7−0.1, G346.6−0.2, CTB 37A, G348.5−0.0, and G349.7+0.2. The infrared colors suggest emission from molecular lines (nine remnants), fine-structure lines (three remnants), polycyclic aromatic hydrocarbons (four remnants), or a combination; some remnants feature multiple colors in different regions. None of the remnants are dominated by synchrotron radiation at mid-infrared wavelengths. The IRAC-detected sample emphasizes remnants interacting with relatively dense gas, for which most of the shock cooling occurs through molecular or ionic lines in the mid-infrared.

Key words: infrared: ISM — shock waves — supernova remnants

Online material: color figure

1. INTRODUCTION

Much of the radiation from supernova remnants (SNRs) is expected to be emitted in the infrared range from heated grains and nebular emission lines. However, SNRs have generally proven to be difficult to detect in the infrared, especially in the Galactic plane, where H II regions are far brighter. Two attempted infrared SNR surveys used *IRAS* observations at 12–100 μm and found possible emission from 12 and 14 remnants (Arendt 1989; Saken et al. 1992), respectively, with only seven in common between the two surveys, from the sample of 95 remnants in the portion of the Galactic plane covered in the new survey presented in this paper.

We present in this paper a new infrared survey of SNRs using the Infrared Array Camera (IRAC; Fazio et al. 2004) on the *Spitzer Space Telescope* (Werner et al. 2004). In the Galactic Legacy Infrared Mid-Plane Survey Extraordinaire (GLIMPSE; Benjamin et al. 2003), the four IRAC arrays—with filters centered at 3.6, 4.5, 5.8, and 8 μm and pixels of $1''.22$ size—were used to map the inner Galaxy within Galactic longitudes $65^\circ > |l| > 10^\circ$ and latitudes $|b| < 1^\circ$. GLIMPSE is a significant advance both because of the large increase in angular resolution and sensitivity and because it covers a new set of infrared wavelengths. There are 95 SNRs within GLIMPSE as per the Green (2004) catalog. The 5 σ sensitivity of GLIMPSE for point sources is 14.0, 12.0, 10.5, and 9.0 mag at 3.6, 4.5, 5.8, and 8 μm, respectively. The raw (1 σ) surface brightness sensitivity is 0.3, 0.3, 0.7, and 0.6 MJy sr^{-1} at 3.6, 4.5, 5.8, and 8 μm, respectively. At 5.8 and 8 μm, most of the Galactic plane is filled with diffuse emission, and at 3.6 and 4.5 μm point-source confusion is significant over much of the Galactic plane. Thus, the primary limitation of this SNR survey is not instrumental noise but rather confusion from other, overlapping astronomical sources.

2. INFRARED EMISSION FROM SUPERNOVA REMNANTS

To provide a basis for the comparison and possible classification of the infrared colors, we consider here the emission mechanisms expected to dominate the mid-infrared. Figure 2 summarizes the predictions in a color-color diagram.

Shocked gas cools through emission lines, and many important emission lines occur in the mid-infrared. The dominant coolant for shocked molecular gas over a wide range of densities is H_2 line emission. Fast shocks into moderately dense gas (e.g., 100 km s^{-1} shocks into gas with density 10^2–10^3 cm^{-3}) cool via atomic fine-structure lines, for which we used a periodic table for fine-structure lines to determine which should be the brightest

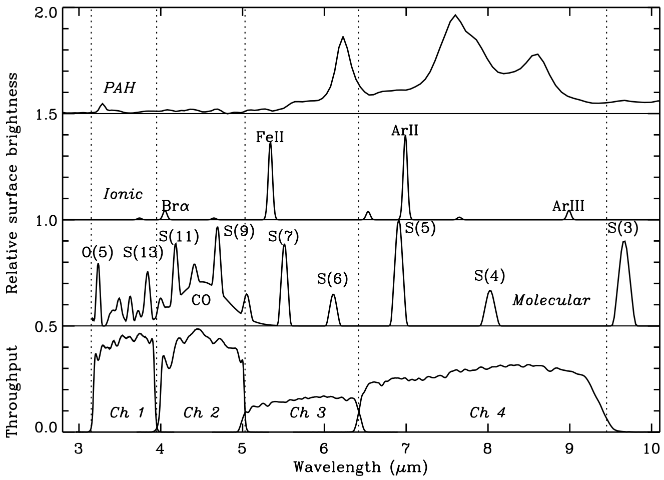

FIG. 1.—*Spitzer* IRAC spectral response compared to three template spectra. The top curve is the *ISO* SWS spectrum of NGC 7023, dominated by PAH emission bands; the second from top is a combination of lines expected from cooling, ionized gas behind a fast shock; the third from top is a combination of H_2 lines and the CO fundamental band. The bottom plot shows the spectral response for each IRAC channel.

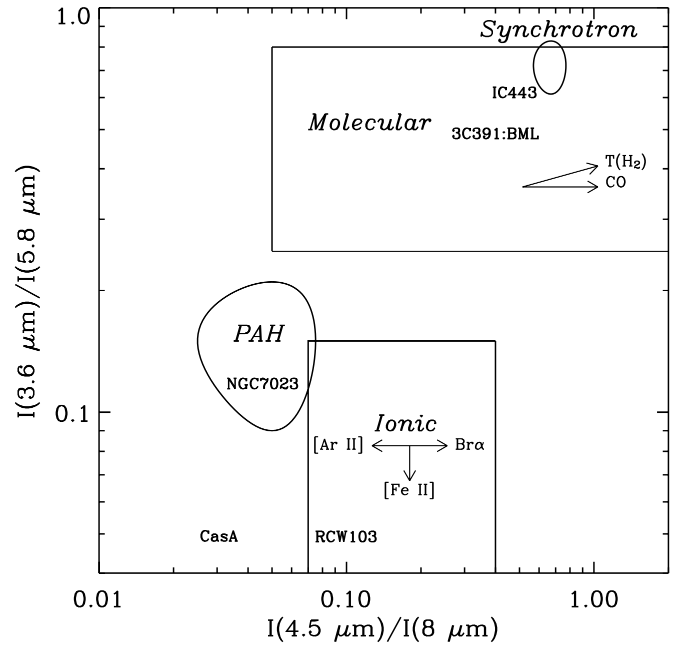

FIG. 2.—Schematic IRAC color-color diagram showing the predicted colors of the main emission mechanisms expected for SNRs in the mid-infrared: shocked molecular gas, shocked ionized gas, and photodissociation regions (PAH). The choice of color axes here separates the major emission mechanisms best. The boundaries delineate the approximate area occupied by a set of models for H_2 excitation and the colors inferred from the observed spectra of photodissociation regions and ionic shocks. For molecular shocks two arrows indicate the color trends for increasing H_2 excitation, $T(H_2)$ and CO vibrational emission. For ionic shocks, the arrows show the color trends of increasing Brα 4.05 μm, [Fe II] 5.35 μm, and [Ar II] 6.99 μm. The boundaries of the various emission mechanisms are intended to bound the expected range of physical conditions behind shock fronts. For the molecular shocks, a range of temperatures from 1000 to 2000 K and mixtures with CO are included. For ionic shocks, line ratios for RCW 103 were used as a basis and supplemented with line ratios for fainter lines in M17. Material with unusual abundances, such as supernova ejecta or circumstellar material, can have unusual colors. Some of the template objects described in the text (reflection nebula NGC 7023 and SNRs Cas A and RCW 103) are plotted at their approximate IRAC colors.

(Reach & Rho 2000). The following lines may be significant (in the indicated channel, with the brightest lines in italics): Pfγ 3.74 μm (channel 1), *Brα 4.05 μm (channel 2),* Pfβ 4.65 μm (channel 2), *Fe II 5.34 μm (channel 3),* Ni II 6.64 μm (channel 4), *Ar II 6.99 μm (channel 4),* Pfα 7.46 μm (channel 4), and Ar III 8.99 μm (channel 4). For the mature SNR 3C 391 with shocks into moderately dense ($n \sim 10^2$ cm^{-3}) gas, the 5–15 μm spectrum showed very bright Fe II and Ar II, in addition to H_2 lines (Reach et al. 2002). For the very young SNR Cas A, which is dominated by ejecta and freshly formed dust, the 6–16 μm spectrum showed very bright Ar II and Ar III (Arendt et al. 1999). For the SNR RCW 103, a wide range of lines was detected over the wavelengths relevant to IRAC: H_2 lines in all channels, Brα in channel 2, Fe II in channel 3, and Ar II and Ar III in channel 4 (Oliva et al. 1999).

Except for the youngest ($<10^3$ yr), SNRs are dominated by swept-up interstellar matter, for which infrared emission from dust is inevitable but the amount and color are not straightforward to predict. Mid-infrared emission from the interstellar medium (ISM) is dominated by polycyclic aromatic hydrocarbon (PAH) bands, especially in the IRAC 5.8 and 8 μm channels. Figure 1 shows the spectrum of the reflection nebula NGC 7023, illustrating how typical interstellar dust may contribute to the IRAC wave bands. Grains are sputtered and vaporized in very strong shocks (Jones et al. 1996), which will reduce the infrared emission per unit mass. More importantly, in attempting to relate infrared features to the SNRs, grains are shattered in strong shocks (Jones et al. 1996). A size distribution with enhanced smaller grains will have a higher color temperature, because the smaller grains are out of thermal equilibrium and emit over a wide range of higher temperatures (Draine & Lee 1984). The smallest grains, or macromolecular PAHs, may be destroyed or altered in even slower shocks and are largely absent in dense, shocked clumps (Reach et al. 2002). Thus, it is nearly impossible to predict the colors of SNRs at IRAC wavelengths: the processes are too complicated (and in competition with each other), and the shocks span too wide a range of properties for there to be a typical color. Diffuse interstellar clouds have a wide range of 12/100 μm ratios, possibly due to shock processing by prior supernova blast waves. Given this range of possible initial conditions of the grains, it is even more unlikely that the processed grains will have predictable properties. That being said, observations of infrared emission from SNRs to date have shown little or no evidence of significant dust emission (PAHs or continuum) within the wavelengths of the IRAC bands. We expect shocked dust to contribute more in the longest wavelength IRAC channel than the others whether the emission is from macromolecular PAHs or from small grains.

Synchrotron emission can contribute to all wavelengths from the radio to X-ray and has been detected in the near-infrared from Cas A (Rho et al. 2003). The color of pure synchrotron emission in the IRAC channels 1/2/3/4 would be approximately 0.6/0.7/0.8/1 (the proportion notation for channels 1/2/3/4, wavelengths 3.6/4.5/5.8/8 μm, is used throughout this paper). None of the SNRs we detected have this color. The one with colors closest to pure synchrotron is for a line of sight for which the mid-infrared spectrum was measured with the *Infrared Space Observatory* (*ISO*) and was dominated by molecular line emission with negligible continuum (Reach & Rho 1999). Since many of the SNRs in our sample are very bright in the radio, we expect them to all have at least faint synchrotron radiation. The expected effect of this synchrotron radiation on the mid-infrared colors is to "fill in" the channels that do not have significant line or dust emission.

Simple models are presented below for the mid-infrared colors expected from the three main SNR emission mechanisms described above. A summary of the derived color/emission mechanism templates is presented in Figure 2.

We now develop simple models to generate template colors for the three main emission mechanisms.

ISM.—First, for the reflection nebula NGC 7023 the colors are 0.054/0.061/0.40/1. For the H II region NRAO 530 (as measured from the GLIMPSE data near the SNR 3C 396), the mid-infrared colors are 0.040/0.046/0.35/1. The origin of these colors is a combination of PAH and nebular line emission, probably with a large PAH contribution based on the similarity to NGC 7023. The H II region and reflection nebula colors are very similar and will be difficult to distinguish, but for our purpose of classifying unprocessed interstellar medium this is not important. Figure 2 shows the colors of NGC 7023 and outlines a region of color-color space that could be attributed to sources with similar spectra.

Shocked molecules.—The colors of a source dominated by molecular emission lines can be estimated using a three-temperature-component H_2 excitation model that matches many lines over a wide range of energy levels for IC 443 (Rho et al. 2001). The IRAC colors of a shocked H_2 clump are expected to be 0.42/0.52/0.90/1. Note the significantly enhanced emission in channels 1 and 2. Furthermore, there is a CO fundamental band that falls within channel 2, with total emission comparable to that of H_2 in Herbig-Haro (HH) shocks with similar densities and shock velocities. Thus, a shocked H_2 + CO clump would have colors 0.42/1/0.90/1. The strong channel 1 + channel 2 enhancement turns out to be a key to distinguishing SNRs interacting with molecular gas from the unrelated interstellar medium or ionized gas.

To allow for variations in the H_2 excitation compared to that seen in IC 443, we computed models for a range of gas temperatures (>1000 K) and combinations of temperature components that yield at least some of the lines observed toward IC 443, RCW 103, or HH objects. The infrared emission of two survey remnants (W44 and 3C 391) for which we have narrowband H_2 images are discussed in § 4, validating the usage of IRAC colors to identify shocked molecular gas.

Ionized gas.—Pure, ionized hydrogen would have IRAC colors of 0.25/3.7/0/1, including the Br and Pf lines listed above, assuming case B recombination at 10^4 K (Osterbrock 1989). However, there will always be some heavier elements in Galactic regions. We consulted a periodic table for fine-structure lines (Reach & Rho 2000) and used the observed line ratios for RCW 103 from spectroscopy with *ISO* (Oliva et al. 1999) as a guide to the brightness relative to Brα. Including lines of H, Fe^+, Ni^+, Ar^+, and Ar^{++}, the predicted colors for ionic shocks are 0.01/0.10/0.74/1. Such gas is distinguishable from unshocked ISM and shocked molecular gas by its bright channel 3 and very faint channel 1. Figure 2 shows the predicted IRAC colors of RCW 103, together with a rectangular region that bounds similar regions. The predicted and observed colors are discussed in the RCW 103 entry in § 4. Note that if the shocks destroy grains more or less efficiently, as in RCW 103, then channel 3 will increase or decrease significantly because Fe II makes the dominant ionic contribution to channel 3.

For stellar ejecta, the colors are more difficult to predict and can have a wide range. The infrared colors of young SNRs are expected to vary from SNR to SNR because the contribution and composition of ejecta depend on a number of physical parameters, such as the type of progenitor star, the amount of the enriched metal abundances, and the degree of particle acceleration. For illustration, the *ISO* spectra of Cas A show little or no [Fe II] emission, which would move sources vertically in Figure 2. And compared to RCW 103, Cas A has little H II emission, which moves points to the left in Figure 2. From archival *ISO* data (including TDT 7510064320), the spectrum of Cas A shows no bright continuum over the IRAC wavelengths and only one bright line ([Ar II] 6.99 μm); the IRAC colors based on the detected spectral lines would be 0.01/0.03/0.18/1, with the paucity of channel 1 and 2 emission due to no bright ionic lines in channel 1 and little expected Brα in channel 2 (due to low H abundance). In Figure 2 the Cas A spectrum falls to the left of the "ionic" region but below the "PAH" region. None of the SNRs we detected in this survey have the colors of synchrotron emission.

The infrared emission of the survey remnants 3C 391, W44, 3C 397, and W49B, for which we have narrowband images in near-infrared Fe II and H_2 filters, is discussed in § 4, validating the use of IRAC colors to identify emission from ionic shocks and to distinguish them from molecular shocks.

3. SURVEY FOR INFRARED EMISSION

Table 1 presents the list of SNRs contained within the boundaries of the infrared survey. The survey procedure is depicted in Figure 3. Each remnant was inspected visually on preliminary mosaics generated immediately on release of the data by the *Spitzer* Science Center (SSC). Gray-scale images at 4.5 and 8 μm were displayed with overlaid circles depicting the size and location of each remnant in the Green (2004) catalog. A preliminary score was assigned according to the following scheme: 1 = likely detection (with infrared shells or other structures coinciding with radio, X-ray, or optical structure, often with a color distinct from the diffuse interstellar medium), 2 = possible detection (with some apparent relation between the infrared and radio image but indistinct colors and too much confusion with unrelated emission), 3 = unlikely detection (but so much confusion with unrelated emission that there could be significant unrecognized emission from the SNR), and 4 = not detected. Remnants with scores of 1 or 2 were selected for follow-up, and improved mosaics were generated for fields centered on each remnant. The improved mosaics were generated using the self-calibration mosaic technique, allowing for relative background offsets between images and a flat field for the array to be determined simultaneously with the sky mosaic (Fixsen et al. 2000). Radio images were obtained from the Molonglo Observatory Synthesis Telescope (MOST) Supernova Remnant Catalog (MSC; Whiteoak & Green 1996), the NRAO VLA Sky Survey (NVSS; Condon et al. 1998), individual authors for some of the individual remnants described in the detailed notes below, or reprocessed Very Large Array (VLA) archival data for G11.4−0.1, 3C 391, 3C 396, and 3C 397. The radio contours were superposed on the infrared images, both the three-color combination of 3.6 (blue), 4.5 (green), and 8 (red) μm and a monochromatic 5.8 μm image. The revised probability of an infrared counterpart was then determined for each remnant. The score was 1 for cases in which a clear association between the infrared emission and the radio emission could be made even if the association was not detailed, since the infrared morphology rarely matches the radio morphology. The score was 2 for remnants for which there is infrared emission that is suggestive but cannot be convincingly associated with the remnant. Of the 95 remnants within the survey boundary, 18 were detected (score 1) and 17 were too confused (score 2). In this paper we concentrate our discussion on remnants with score 1, but those with score 2 are worthy of future detailed studies.

3.1. *Comparison to Previous Surveys*

For comparison, the *IRAS*-based survey by Arendt (1989) detected 12 (17%) of the remnants within the portion of the Galactic plane included in GLIMPSE, and the independent *IRAS*-based survey by Saken et al. (1992) detected 14 (18%).

TABLE 1

Supernova Remnants in the IRAC GLIMPSE Survey

SNR	Name	Size (arcmin)	Detected?[a]	SNR	Name	Size (arcmin)	Detected?[a]
G11.2−0.3		4	1	G308.1−0.7		13	4
G11.4−0.1		8	3	G308.8−0.1		25	2
G12.0−0.1		7	3	G309.2−0.6		14	3
G13.5+0.2		5	3	G309.8+0.0		22	3
G15.9+0.2		6	3	G310.6−0.3	Kes 20B	8	2
G16.7+0.1		4	3	G310.8−0.4	Kes 20A	12	1
G18.8+0.3	Kes 67	14	3	G311.5−0.3		5	1
G20.0−0.2		10	3	G312.4−0.4		38	3
G21.5−0.9		4	3	G315.4−0.3		19	2
G21.8−0.6	Kes 69	20	1	G315.9−0.0		10	3
G22.7−0.2		26	1	G316.3−0.0	MSH 14−57	20	3
G23.3−0.3	W41	27	2	G317.3−0.2		11	3
G23.6+0.3		10	3	G318.2+0.1		37	3
G24.7+0.6		21	3	G318.9+0.4		20	3
G24.7−0.6		15	4	G321.9−0.3		27	3
G27.4+0.0	4C −04.71	4	3	G322.5−0.1		15	3
G27.8+0.6		39	3	G323.5+0.1		13	2
G28.6−0.1		11	3	G327.4+0.4	Kes 27	21	2
G29.6+0.1		5	4	G328.4+0.2	MSH 15−57	5	4
G29.7−0.3	Kes 75	3	3	G329.7+0.4		36	2
G31.5−0.6		18	3	G332.0+0.2		12	4
G31.9+0.0	3C 391	6	1	G332.4−0.4	RCW 103	10	1
G32.1−0.9		40	3	G332.4+0.1	Kes 32	15	2
G32.8−0.1	Kes 78	17	3	G335.2+0.1		21	2
G33.2−0.6		18	3	G336.7+0.5		12	4
G33.6+0.1	Kes 79	10	2	G337.0−0.1	CTB 33	2	3
G34.7−0.4	W44	31	1	G337.2−0.7		6	4
G36.6−0.7		25	2	G337.8−0.1	Kes 41	7	2
G39.2−0.3	3C 396	7	1	G338.1+0.4		15	4
G40.5−0.5		22	4	G338.3−0.0		8	3
G41.1−0.3	3C 397	4	1	G338.5+0.1		9	3
G42.8+0.6		24	4	G340.4+0.4		8	4
G43.3−0.2	W49B	4	1	G340.6+0.3		6	2
G45.7−0.4		22	2	G341.2+0.9		19	4
G46.8−0.3		15	3	G341.9−0.3		7	4
G49.2−0.7	W51C	30	3	G342.0−0.2		10	3
G54.1+0.3		2	3	G342.1+0.9		9	4
G54.4−0.3		40	1	G343.1−0.7		24	3
G55.0+0.3		17	2	G344.7−0.1		10	1
G57.2+0.8		12	4	G345.7−0.2		6	4
G59.5+0.1		5	3	G346.6−0.2		8	1
G296.1−0.5		32	3	G347.3−0.5		60	3
G296.8−0.3		16	3	G348.5+0.1	CTB 37A	15	1
G298.5−0.3		5	2	G348.5−0.0		10	1
G298.6−0.0		11	2	G348.7+0.3	CTB 37B	17	3
G299.6−0.5		13	3	G349.2−0.1		8	3
G302.3+0.7		17	3	G349.7+0.2		2	1
G304.6+0.1	Kes 17	8	1				

[a] Likelihood of mid-infrared counterpart for the SNR, determined by inspection of the IRAC data and comparison to existing radio images: 1 = detected (18 objects), 2 = possibly detected but confused (17 objects), 3 = not detected but confused (44 objects), and 4 = not detected at GLIMPSE sensitivity (16 objects).

Only seven (10%) of these remnants were detected in common by the two *IRAS*-based surveys: 3C 391, W49B, G54.1+0.3, Kes 17, G315.4−0.3, G340.6+0.3, and G349.7+0.2. The new *Spitzer* IRAC results presented here are a significant advance, primarily because of the increase in angular resolution, which allows a better separation of stars, H II regions, and other interstellar clouds from the remnants. The present survey detects six remnants in common with Arendt (1989) and four remnants in common with Saken et al. (1992). There are only four remnants in common among all three infrared surveys: 3C 391, W49B, Kes 17, and G349.7+0.2.

First, let us consider those SNRs apparently detected by *Spitzer* and *IRAS*. We compared the GLIMPSE images to the *IRAS* images from the Arendt (1989) catalog. The *IRAS* images of W44, W49B, and G349.7+0.2 contain emission plausibly associated with the remnant as traced by radio and *Spitzer* infrared images. For 3C 391, the 60 μm emission shows a believable emission peak from the remnant, while the other channels are clearly due to unrelated H II regions. For Kes 17 and G11.2−0.3, the structures in the *IRAS* images all appear to be due to unrelated H II regions, and their apparent detections are spurious. The dashed circles in the plates of Arendt's (1989) survey indicate

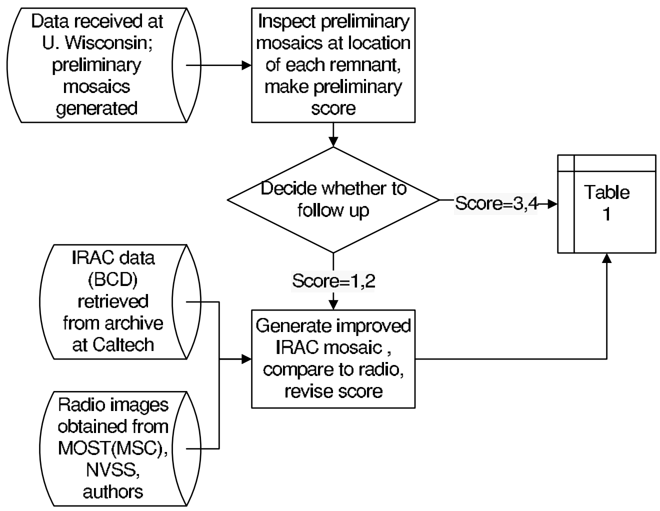

Fig. 3.—Flowchart of the GLIMPSE Galactic plane SNR survey.

the region within which he measured fluxes; they often contain bright H ii regions, well-resolved in the new *Spitzer* images that are clearly outside the radio shells.

As for the SNRs apparently detected by *IRAS* and not *Spitzer*, they are either so confused with H ii regions (e.g., G12.0−0.1) that we cannot tell whether there are counterparts in either survey, or the *IRAS* detections (e.g., CTB 37B) are likely to be unrelated H ii regions. In principle, some of the mismatches between *IRAS* and *Spitzer* could be due to the difference in wavelength, since it is possible that the *IRAS* emission is from dust while *Spitzer* IRAC traces shocked gas; however, for the specific cases in the present survey, we attribute the differences between the *IRAS* and *Spitzer* surveys to be primarily due to contamination of the *IRAS* observations at low Galactic latitudes. Other infrared surveys with higher angular resolution, for example, 24 μm observations with *Spitzer* and future far-infrared observations with the *Herschel Space Observatory*, will likely detect many more counterparts.

4. RESULTS FOR INDIVIDUAL REMNANTS

Table 2 lists the 18 remnants detected by GLIMPSE. Brief descriptions of the mid-infrared emission, and some relevant context, are given below for each detected remnant, with detected (score 1) remnants in bold and possibly detected (score 2) remnants in italics.

G11.2−0.3: This compact, circular SNR has a composite radio morphology with a clearly defined, steep-spectrum shell (brightest in the southeast) combined with a flat-spectrum core. X-ray observations show a shell (with a thermal spectrum) similar to that seen in the radio; a centrally located pulsar (AX J1811.5−1926) and a pulsar wind nebula are associated with the SNR (Kaspi et al. 2001). Some evidence indicates that G11.2−0.3 is associated with the supernova of 386 AD, and the expansion of the remnant was detected by proper motion of the radio shell (Tam & Roberts 2003); both these factors suggest that this SNR is relatively young. The mid-infrared images (Fig. 4, *left*) reveal a thin filament with three bright segments located within the southeastern rim of the SNR. Figure 4 (*right*) shows that the filaments correspond precisely with the two brightest segments of the southeastern X-ray rim. The filaments connect to a fainter extension along most of the eastern radio shell. More diffuse infrared emission is seen toward the eastern half of the SNR, although it is unclear whether this emission is in fact associated with the SNR. No infrared emission is seen toward the northwestern quadrant

TABLE 2

Properties of Detected Supernova Remnants[a]

SNR	Name	Diameter (arcmin)	Region	3.6/8	4.5/8	5.8/8	$I8$ (MJy sr^{-1})
G11.2−0.3		4	Southeastern rim	0.34	0.48	0.58	7.5
G21.8−0.6	Kes 69	20	Southern ridge	<0.14	0.91	1.4	2
G22.7−0.2		26	Southern boundary	<0.07	<0.07	0.37	23
G31.9+0.0	3C 391	6	BML/OH maser	0.18	0.36	0.67	23
			Northwestern Fe/radio bar	<0.14	0.41	1.7	5
G34.7−0.4	W44	31	Eastern shell	0.37	0.75	0.75	11
G39.2−0.3	3C 396	7	Western shell	<0.10	0.27	0.63	10
			Central filament	<0.07	0.04	0.37	27
G41.1−0.3	3C 397	4	Northern shell	<0.07	0.14	0.73	8
G43.3−0.2	W49B	4	Fe/radio hoop	0.08	0.46	1.0	8
			H_2 filament	0.16	0.42	0.76	6
G54.4−0.3		40	Northern boundary	0.04	0.04	0.33	15
G304.6+0.1	Kes 17	8	Filament	0.33	0.34	0.67	5
			Shell	0.12	0.30	0.39	29
G310.8−0.4	Kes 20A	12	Southeastern shell	0.18	0.18	0.61	15
G311.5−0.3		5	Shell	0.41	0.54	0.91	9
G332.4−0.4	RCW 103	10	Shell	0.19	0.38	0.79	15
			Filament	<0.07	0.14	0.59	10
G344.7−0.1		10	Shell	<0.20	0.23	0.82	10
G346.6−0.2		8	Shell	0.23	0.41	0.61	6
G348.5+0.1	CTB 37A	15	Northern blob	0.11	0.32	0.52	24
			Arc	0.07	0.04	0.42	62
G348.5−0.0		10	Filament	0.14	0.29	0.64	14
G349.7+0.2		2	Filament	0.05	0.14	0.59	170

[a] The columns 3.6/8, 4.5/8, and 5.8/8 are the ratios of the surface brightness in IRAC channels 1, 2, and 3 to IRAC channel 4. The emission was assumed to be spatially extended, so the colors measured from the images were multiplied by factors of 1.36, 1.36, and 0.91, respectively (Reach et al. 2005b).

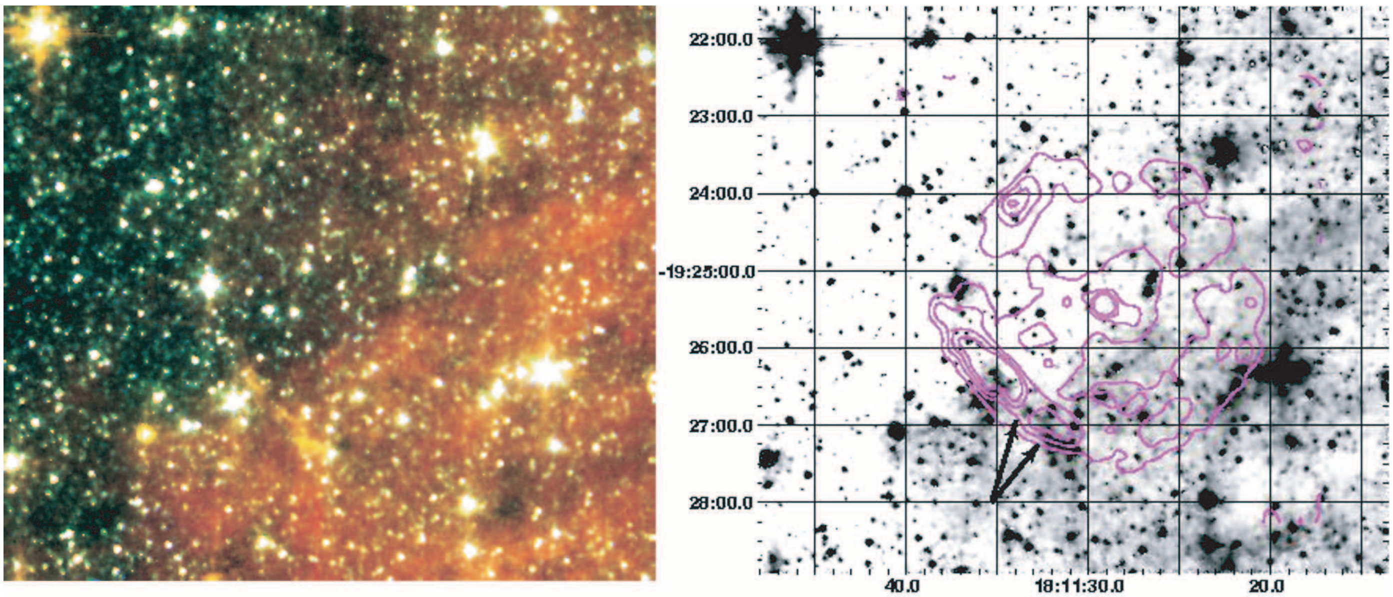

FIG. 4.—*Left*: *Spitzer* IRAC color image of the SNR G11.2−0.3. The colors are red = 8 μm, yellow = 5.8 μm, green = 4.5 μm, blue =3.6 μm, and magenta = (5.8 μm) − [0.32(8 μm)]. These IRAC images were adaptively smoothed to reduce noise while preserving angular resolution on bright features. *Right*: *Spitzer* IRAC 5.8 μm image of the SNR G11.2−0.3. *Chandra* all-energy contours are superposed. Two infrared filaments are indicated (*arrows*).

of the SNR. There is no infrared emission associated with the pulsar wind nebula. The filament near $\alpha = 18^{\rm h}11^{\rm m}35\overset{\rm s}{.}0$, $\delta = -19°26'23''$ is detected in channels 3 and 4 with comparable brightness in both channels (10 MJy sr^{-1}), but it is not seen in channels 1 or 2. The blob of emission at $\alpha = 18^{\rm h}11^{\rm m}31\overset{\rm s}{.}5$, $\delta = -19°27'16''$ is detected in all four IRAC channels, with color ratios 0.3/0.7/1.1/1. The colors suggest that the IRAC emission from the filaments is dominated by line emission from shocked gas and certainly not the PAH dust that dominates unshocked ISM. Since the remnant is young, some of the emission could also arise from ejecta.

Kes 69 (G21.8−0.6): Figure 5 shows a prominent, "green" ridge of mid-infrared emission passing through $\alpha = 18^{\rm h}30^{\rm m}22\overset{\rm s}{.}0$, $\delta = -10°15'41''$ in the southern radio shell. The IRAC color ratios are (<0.1)/0.67/1.5/1, which are inconsistent with PAH emission. Channels 2 and 3 are most likely dominated by lines from shocked gas. The exceptionally bright channel 3 emission (relative to channel 4) could be due to a bright Fe II line, suggesting very efficient grain destruction in the shocks. The bulk of the radio emission of Kes 69 originates from the southeastern shell; likewise, the infrared emission originates from the same location. The X-ray emission, on the contrary, appears interior to the radio shell (Yusef-Zadeh et al. 2003). An OH maser has been detected from the northern part of Kes 69 (Green et al. 1997; Yusef-Zadeh et al. 2003); faint, diffuse, mid-infrared emission, possibly unrelated to the SNR, is seen in the vicinity of the OH maser.

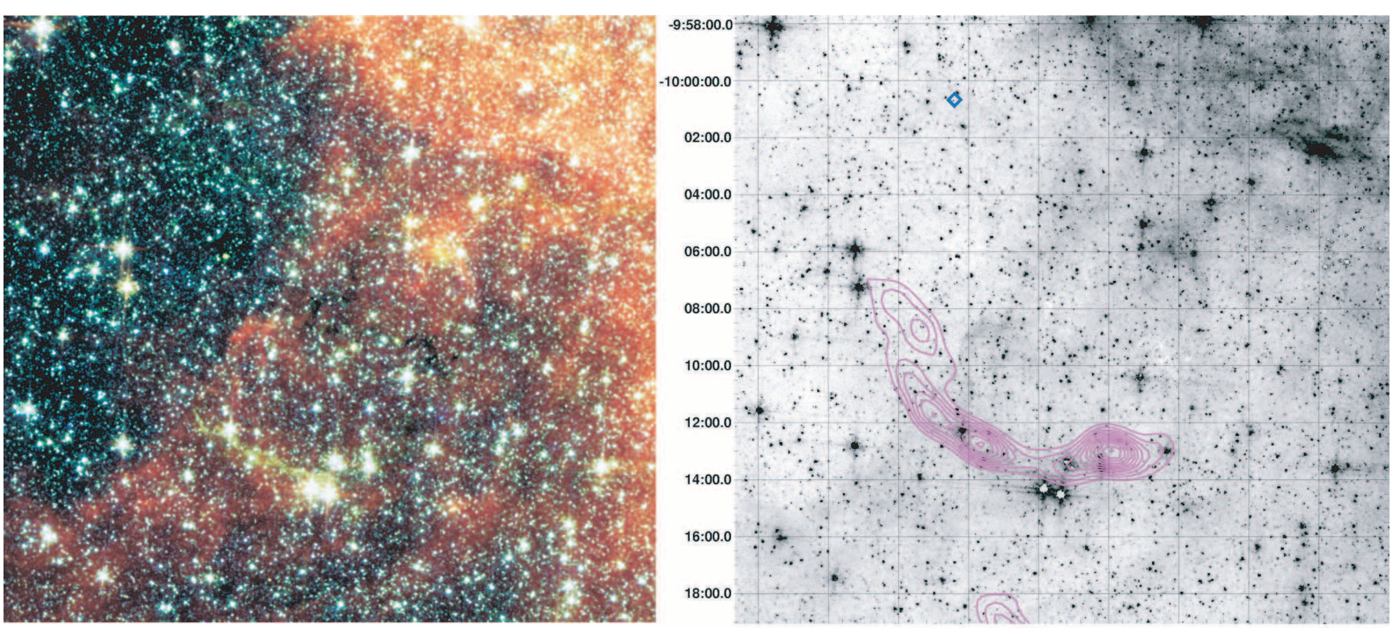

FIG. 5.—*Left*: *Spitzer* IRAC color image of the SNR Kes 69. The colors are red = 8 μm, yellow = 5.8 μm, green = 4.5 μm, and blue = 3.6 μm. *Right*: *Spitzer* IRAC 5.8 μm image of Kes 69 with radio (NVSS) contours superposed. The diamond in the northwest is the position of an OH 1720 MHz maser.

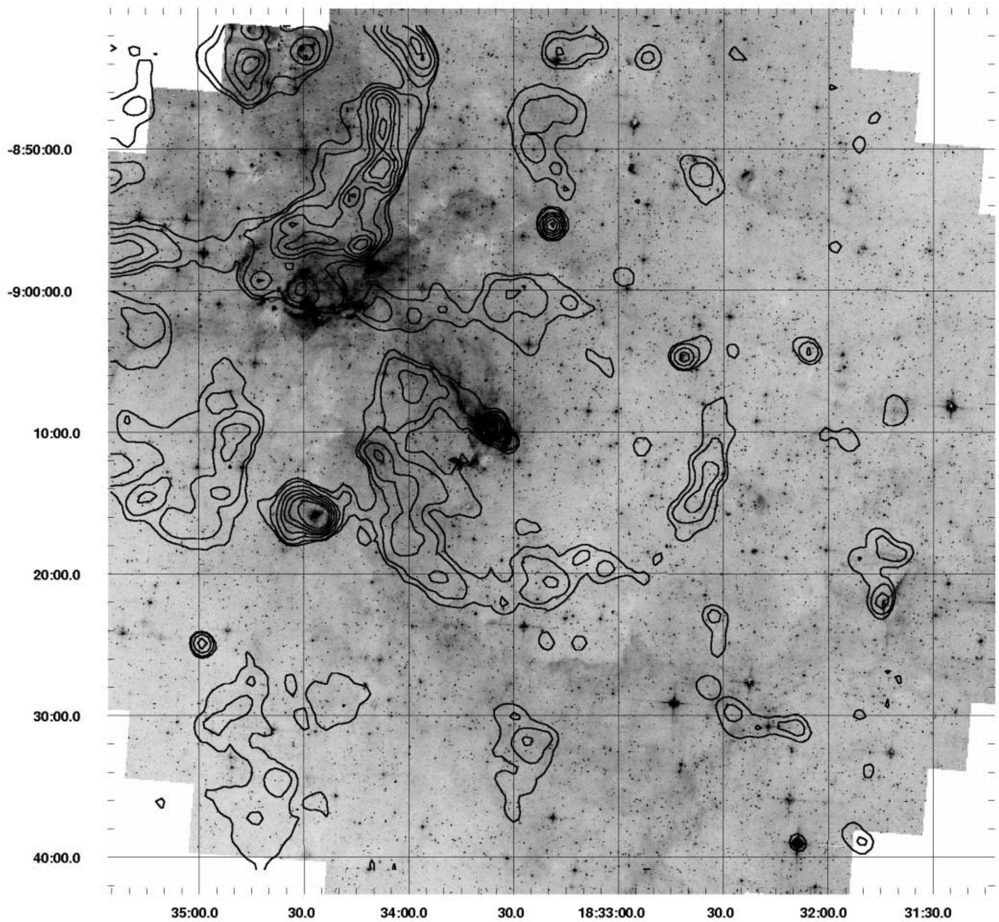

FIG. 6.—*Spitzer* IRAC 5.8 μm image of the SNR G22.7−0.2, with radio contours from the NVSS. W41 is in the upper left of this image.

G22.7−0.2: This remnant is located in a field with multiple H II regions and is adjacent to W41. A very bright infrared region G22.75−0.25 ($\alpha = 18^h33^m46\overset{s}{.}5$, $\delta = -09^\circ10'02''$) is located just east of the center of the remnant. This region is evident as a very bright compact source in the 1420 MHz NVSS (Condon et al. 1998) with flux ~100 mJy, but the source is not evident at 330 MHz (Kassim 1992), suggesting that it may be thermal emission from an H II region. Elsewhere along the SNR shell there is a small probable H II region in the northeast at G22.73−0.01 ($\alpha = 18^h32^m42\overset{s}{.}3$, $\delta = -09^\circ04'43''$). A relatively unique region is located in the western shell at G22.78−0.40 ($\alpha = 18^h34^m12\overset{s}{.}7$, $\delta = -09^\circ11'15''$). There are numerous mid-infrared filaments evident at 5.8–8 μm, and at least one with relatively bright 3.6–4.5 μm emission. The infrared emission is probably a mixture of PAH features and gas lines. The positional coincidence with the radio shell, filamentary morphology, and infrared colors led us to suspect that this is a supernova-cloud interaction region, but improved infrared images or other supporting evidence are needed to properly classify the nature of this region. There is a bright region of infrared emission between G22.7−0.2 and the adjacent SNR W41. While this could be a coincidental projection effect, the location is very suggestive. This could be a case in which an interstellar cloud is being "sandwiched" by impacts from different SNRs (or the progenitors' and cluster members' winds) on either side. There is a general "deficit" of infrared emission within the radio shell, clearly evident in Figure 6. The region of decreased infrared emission has a sharp boundary in the southern portion of the remnant, just south of the NVSS radio contours. The shape of the southern cavity boundary follows the shape of the remnant too closely to be a chance alignment. The colors of this southern rim are very red, possibly due to PAH emission. The morphology and colors suggest that the observed emission is not from strong shocks; instead, it may arise from a region evacuated by the progenitor (and possibly other cluster members) and currently illuminated by the remaining cluster members.

W41 (G23.3−0.3).—This SNR is located in an incredibly rich field of infrared emission, with a large H II region and embedded cluster ($\alpha = 18^h34^m47\overset{s}{.}3$, $\delta = -08^\circ32'56''$) in the northern shell, diffuse red emission throughout the entire region, a dark lane running roughly north-south through the entire SNR, numerous compact H II regions and small shells, and extremely red sources that are probably protostars. Some of these objects may be related to the SNR progenitor's cluster. No detailed association between specific infrared features and the SNR was noticed (but see the discussion of G22.7−0.2 above).

3C 391 (G31.9+0.0): Figure 7 shows the IRAC images of 3C 391. This remnant was previously observed in the mid- and far-infrared using *ISO*: molecular and ionic lines include H_2, OH, H_2O, CO, [O I], and [O III] (Reach & Rho 1998, 2000), and near-infrared imaging reveals shocked H_2 and [Fe II] emission (Reach et al. 2002). In Figure 7 (*left*), two green (channel 2) patches are evident; they are located at the northern and southern terminus of the bright radio semicircular radio shell. The southern one comprises the "broad molecular line" (BML) region 3C 391:BML ($\alpha = 18^h49^m23\overset{s}{.}1$, $\delta = -00^\circ57'38''$), where bright near-infrared H_2 emission and broad millimeter-wave molecular

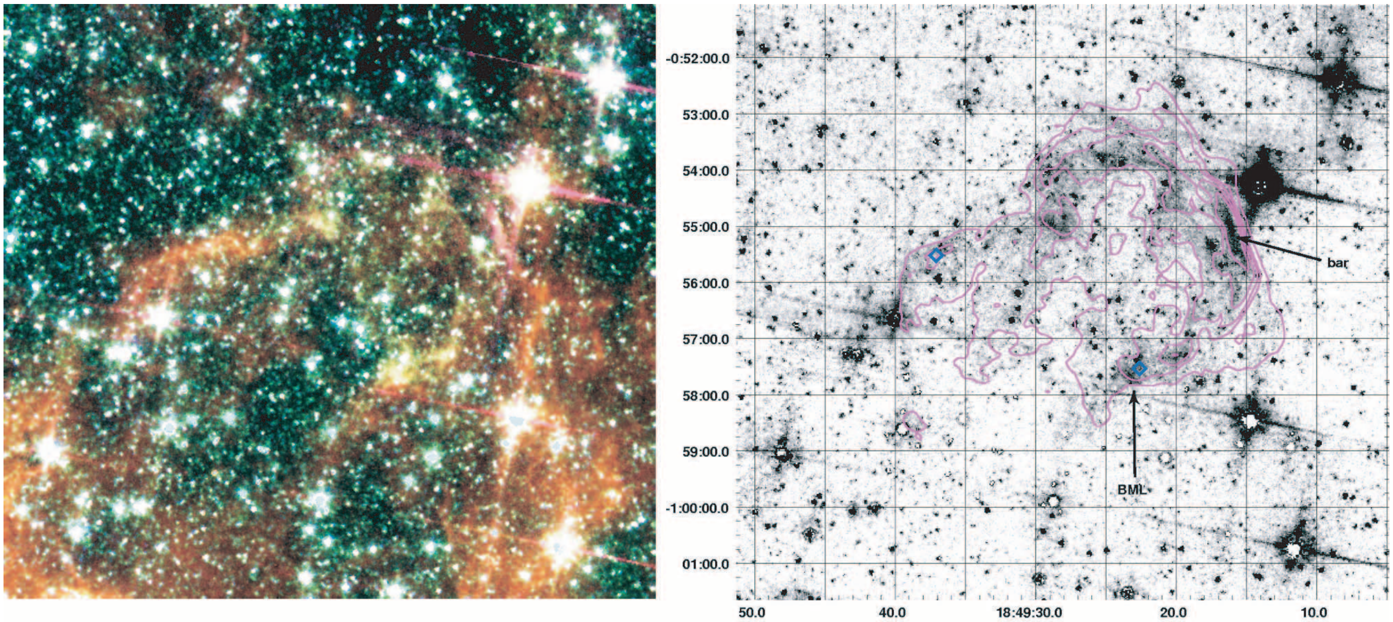

FIG. 7.—*Left*: *Spitzer* IRAC color image of the SNR 3C 391. The colors are red = 8 μm, green = 4.5 μm, blue = 3.6 μm, and magenta = (5.8 μm) − [0.308(8.0 μm)]. *Right*: *Spitzer* IRAC 5.8 μm image minus a scaled 8 μm image to suppress emission with colors of normal ISM. The radio contours (*magenta*) were constructed from VLA 20 cm data at 16″ resolution (Brogan et al. 2005). The two OH masers are indicated with blue diamonds, and two features discussed in the text—the BML region and the radio bar—are labeled.

lines were previously detected (Reach et al. 2002); it also includes one of the two 1720 MHz OH masers spots associated with 3C 391 (Frail et al. 1996). The IRAC color ratios for 3C 391:BML are consistent with shocked molecular gas. The northern patch ($\alpha = 18^{\mathrm{h}}49^{\mathrm{m}}28\overset{\mathrm{s}}{.}8$, $\delta = -00°55'00''$) also has associated near-infrared H_2 emission in a test image taken at Palomar (Reach et al. 2005a); reanalysis of the CO and CS spectra reveals no broad molecular lines at this position. In addition to these patches, fainter and more extensive emission is evident in channels 2, 3, and 4, extending around the horseshoe-shaped radio shell.

The northwestern bar, where the brightest part of the radio shell is tangential to a giant molecular cloud, is detected in IRAC channels 2, 3, and 4 and is particularly bright in channel 3. This bar has very bright near-infrared 1.64 μm [Fe II] emission (Reach et al. 2002), and IRAC channel 3 contains the 5.34 μm line of [Fe II], whose upper energy level is the same as the lower energy level of the 1.64 μm; the 5.34 μm transitions should have at least comparable flux (and potentially much higher if the gas is cooler than 5000 K). If we interpret the IRAC channel 3 emission from the bar as entirely from the 5.34 μm line, its surface brightness is 2×10^{-3} ergs cm^{-2} s^{-1} sr^{-1}, while the 1.644 μm line brightness at the same position is 1×10^{-4} ergs cm^{-2} s^{-1} sr^{-1}; this line ratio can be reproduced if the shocked gas has $T \sim 2200$ K (for $n \sim 10^2$ cm^{-3}), which is entirely plausible for the fast J-type shocks inferred for this location. Thus, for the bright northwestern bar, IRAC channel 3 is likely to be [Fe II] line emission. Some contribution from Ar would be expected from such shocks in IRAC channel 4: the *ISO* ISOCAM 12–18 μm image was interpreted as a sum of the [Ne II] and [Ne III] lines, and the situation should be similar for IRAC channel 4 containing [Ar II] and [Ar III]. Comparing the ISOCAM 12–18 μm and IRAC channel 4 images, the inferred ratio ([Ne II] + [Ne III])/([Ar II]+]Ar III]) ~ 2, which again is plausibly explained by shocked gas with abundances and excitation conditions as described by Reach et al. (2002).

Thus, for 3C 391 we find significant infrared emission correlated with the radio shell but with distinct colors: the "green" (enhanced channel 2) regions are associated with near-infrared emission from H_2 and originate from shocked molecular gas, while the "magenta–red" regions (enhanced channel 3) have associated near-infrared [Fe II] and originate from shocked, ionized gas.

Kes 79 (G33.6+0.1).—Kes 79 was cataloged as a possible mixed-morphology SNR with centrally filled X-rays detected by the *ROSAT* PSPC surrounded by a well-defined radio shell (Rho & Petre 1998). There is extensive mid-infrared emission near this SNR, with some features possibly at the distance of the remnant but no clear evidence for emission from shock fronts. Interestingly, there is an infrared dark cloud located near the eastern boundary of the SNR for which CO observations suggest interaction with molecular clouds, although broad molecular lines were not detected (Green & Dewdney 1992). There are a number of point sources within the dark clouds with infrared colors consistent with those of protostars, and there are also a number of small diffuse structures similar to ultracompact H III regions. No infrared point source coincides with the compact central object (Seward et al. 2003).

W44 (G34.7−0.4): W44 is a mixed-morphology SNR featuring centrally filled, thermal X-ray emission surrounded by a well-defined radio shell (Rho et al. 1994). The detections of broad molecular lines and shocked H_2 emission (Reach et al. 2005a and references therein) unambiguously show that the remnant is interacting with molecular clouds. The *Spitzer* color image of W44 in Figure 8 is one of the best images from this survey. A large, green, elliptical shell matches the radio shell rather closely. In particular, the IRAC channel 2 image emission is almost identical to the near-infrared H_2 images taken for the fields toward the northeastern and southern portions of the shell (Reach et al. 2005a), indicating that this emission is from shocked H_2. This is also consistent with the line contribution we estimated based on the color ratio of the four channels described in § 2 and validates our predicted IRAC colors for molecular shocks. There is an infrared-dark cloud at the boundary of the eastern shell of W44. The patch of red emission south of the dark cloud is likely a small H II region based on the ratio of Hα and [S II] (Rho et al. 1994). The IRAC channel 3 image is similar to the channel 2 image, as expected because bright H_2 lines in channel 2 will always be accompanied by bright lines

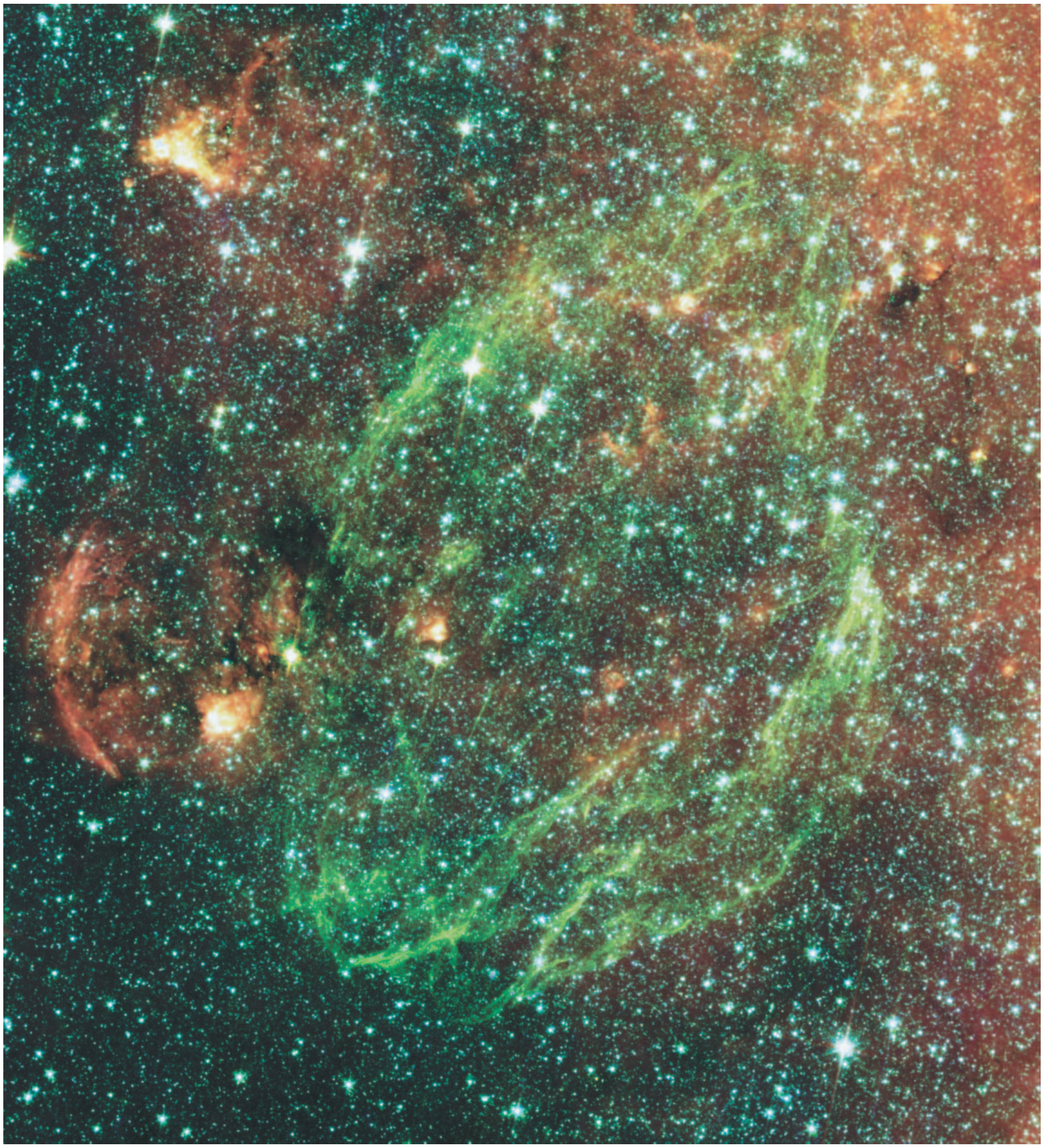

FIG. 8.—*Spitzer* IRAC color image of W44. The SNR appears "green" in the IRAC colors because channel 2 is relatively much brighter in the SNR shell than in the surrounding ISM (including both the surrounding molecular cloud and the H II regions to the east and northeast).

in channel 3. But channel 3 is mixed with the eastern H II region and other ISM emission outside the remnant. The remnant is barely noticeable in IRAC channel 4 due to confusion with unrelated emission.

G36.6−0.7.—There is a possible shell of infrared emission bounding the SNR toward the north, as well as a dark filament in the north and clumps in the west and southwest. There is no clear evidence for emission from shock fronts.

3C 396 (G39.2−0.3): Infrared emission is detected from this remnant in three forms. First, faint, filamentary emission is detected in the western radio shell of this remnant, with IRAC colors clearly distinct from normal interstellar emission. In Figure 9 (*left*), the western shell appears green; a cut through the western shell near $\alpha = 19^{\rm h}03^{\rm m}56\overset{\rm s}{.}3$, $\delta = +05°25'46''$ yields IRAC colors (<0.08)/0.2/0.69/1, suggesting emission from shocked, ionized gas.

Second, there are two very bright infrared filaments, at $\alpha = 19^{\rm h}04^{\rm m}18\overset{\rm s}{.}5$, $\delta = +05°20'33''$ and $\alpha = 19^{\rm h}04^{\rm m}17\overset{\rm s}{.}0$, $\delta = +05°27'07''$ (each $\sim 30''$ long), just inside the eastern radio shell. The filaments are clearly separated from the recently detected pulsar wind nebula (Olbert et al. 2003) and are located within a region of exceptionally high radio polarization. We suspect that these bright filaments, which are highly unusual, are part of the SNR, which is the only known structure in the interstellar medium at that location. The color ratios of the filaments are (<0.05)/0.03/0.4/1, at a location at which the 8 μm surface brightness is 30 MJy sr^{-1}. These colors are similar to normal interstellar medium, so the filaments could be photodissociation regions (e.g., compressed filaments that were shocked long ago, rather than active shock fronts).

Finally, there is faint, diffuse emission surrounding the entire radio shell, with some bright, extended regions just outside the eastern periphery. The "blowout tail" discussed by Patnaik et al. (1990) from radio data extends eastward from the remnant and wraps north then back over the top of the remnant. In the infrared, the "tail" starts with a bright region at $\alpha = 19^{\rm h}04^{\rm m}26\overset{\rm s}{.}0$, $\delta = +05°27'55''$ that is connected to an intricate set of infrared filaments that follow the radio structure, with the infrared region

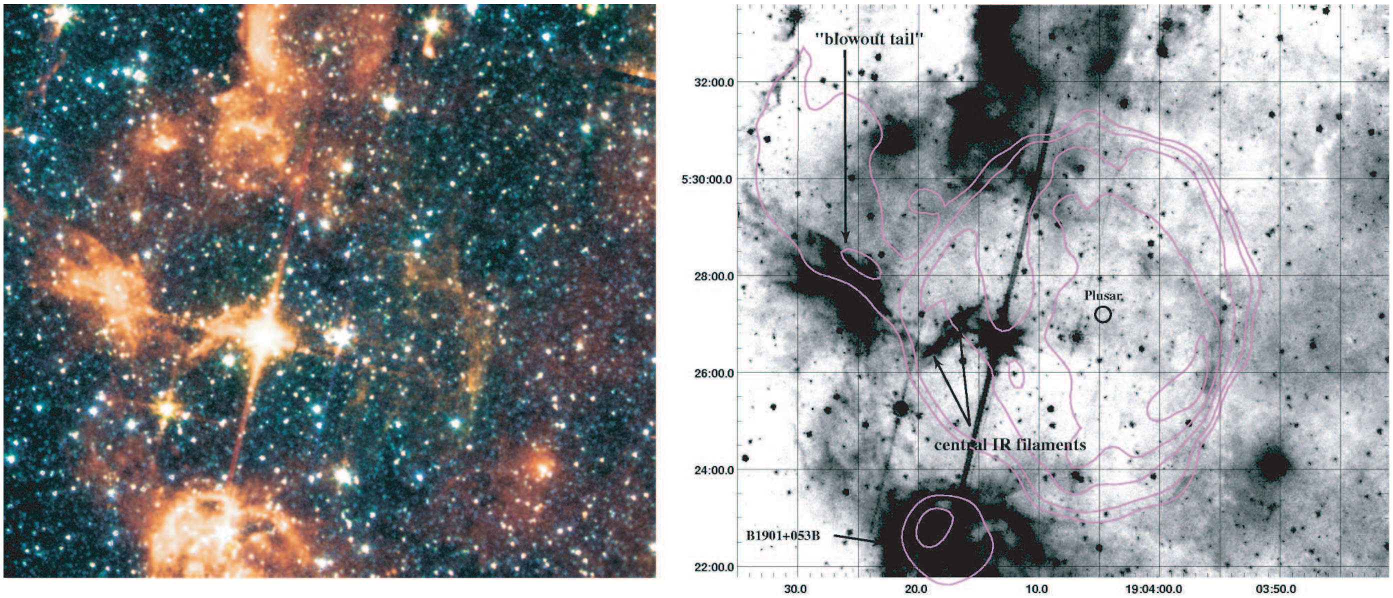

FIG. 9.—*Left*: *Spitzer* IRAC color image of the SNR 3C 396 (G39.2−0.3). The colors are red = 8 μm, yellow = 5.8 μm, green = 4.5 μm, and blue = 3.6 μm. *Right*: *Spitzer* IRAC 8 μm image of the SNR 3C 396 (G39.2−0.3), with radio contours overlaid. The infrared gray scale is logarithmic. The radio image was generated using 20 cm images from the VLA archive; contours levels are 1.5, 4.2, 12, 26, and 45 mJy beam^{-1} (with 15″ resolution). Features discussed in the text are labeled.

displaced somewhat southward. While this "tail" could be an H II region, the remarkably high radio polarization (50%) suggests that most of the radio emission is synchrotron radiation. Thus, the "tail" could be due to energetic particles in a plume extending through the "hole" in the eastern shell of the remnant. The bright infrared region near the base of the "tail" is detected only in channels 3 and 4, with a ratio 0.3:1 consistent with photodissociation regions or H II regions.

3C 397 (G41.1−0.3): This small remnant has faint mid-infrared emission that clearly correlates with portions of the radio shell. Figure 10 shows relatively distinct filaments near $\alpha = 19^{\rm h}07^{\rm m}40\overset{\rm s}{.}5$, $\delta = +07°08'48''$. The infrared emission was detected in channels 2, 3, and 4, with ratios 0.1/0.8/1 (for channels 2/3/4) that are inconsistent with photodissociation regions and H II regions but are plausible for fine-structure lines from shocked gas. The high 5.8 μm brightness could be due to efficient grain destruction leading to a bright Fe II 5.3 μm line.

W49B (G43.2−0.2): W49B has a relatively unique structure, with its radio emission forming a set of curved filaments in either a spiral or barrel-hoop morphology (Moffett & Reynolds 1994). The X-ray emission is thermal with rich line emission, mostly attributed to ejecta material, indicating that it is a rather

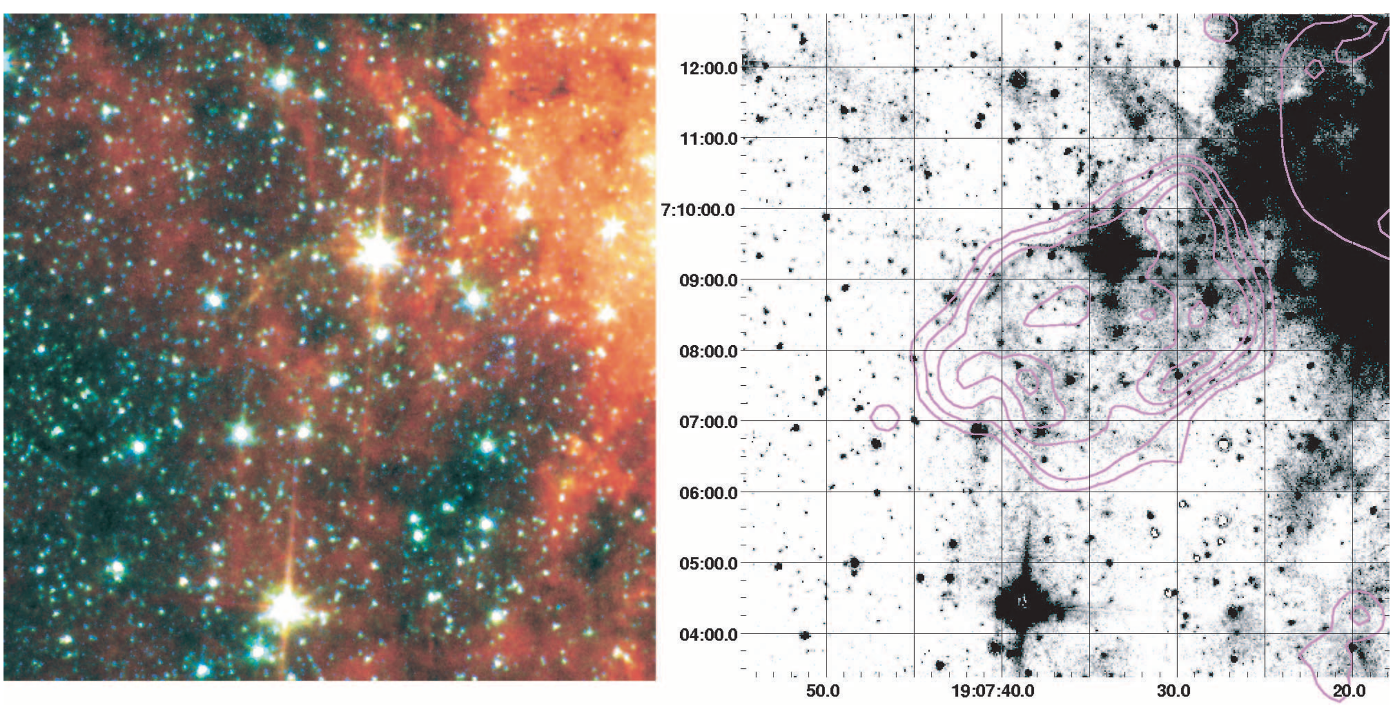

FIG. 10.—*Spitzer* IRAC color image (*left*) and 5.8 μm image of 3C 397 with radio contours overlaid (*right*). The infrared gray scale is logarithmic. The radio image was generated using 20 cm images from the VLA archive; contours levels are 10, 46, 83, and 120 mJy beam^{-1} (with ~15″ resolution).

FIG. 11.—*Spitzer* IRAC color image of the SNR W49B, with red = 8 μm, green = 4.5 μm, blue = 3.6 μm, and magenta = 5.8 μm minus a scaled 8 μm image. There are two distinct types of emitting region: the molecular emission is green and is brighter at the eastern and southwestern extremities, while the ionic emission is magenta and is brighter in the radio "loops."

young SNR (Hwang et al. 2000). The SNR is clearly detected in the GLIMPSE images. Figure 11 shows the IRAC color image, with the emission from the SNR clearly dominating over other nearby diffuse emission. There are two very distinct colors (Fig. 11, *green and magenta*). Much of the SNR has a filamentary structure, and this part of the IRAC image closely follows the radio morphology, with its series of loops. These appear relatively "magenta" in Figure 11 due to very bright emission in channel 3. The color ratios toward a radio and near-infrared [Fe II] filament near $\alpha = 19^{\rm h}11^{\rm m}07\overset{\rm s}{.}0$, $\delta = +09^\circ07'01''$ (Table 2) suggest line emission from ionic shocks. Another distinct component of the infrared emission, forming a sort of outer shell toward the east and southwest, appears relatively "green" in Figure 11; the colors toward $\alpha = 19^{\rm h}11^{\rm m}14\overset{\rm s}{.}3$, $\delta = +09^\circ04'42''$ (Table 2) are consistent with lines from shocked molecular gas. The presence of these two distinct types of shock was first found in near-infrared, narrowband images, which show [Fe II] 1.66 μm and radio emission distributed like the "magenta" emission in Figure 11 and H_2 2.12 μm emission distributed like the "green" emission in Figure 11 (Keohane et al. 2005). This remnant, together with 3C 391, serves as an empirical validation of the IRAC color interpretations in this paper using near-infrared narrowband imaging.

G45.7−0.4.—There is an infrared filament approximately parallel to part of the radio shell around $\alpha = 19^{\rm h}16^{\rm m}36\overset{\rm s}{.}0$, $\delta = +11^\circ08'00''$ and a potentially related arc near $\alpha = 19^{\rm h}16^{\rm m}30^{\rm s}$, $\delta = +11^\circ14'16''$ but no clear evidence for emission from shocked gas or dust.

G54.4−0.3: The cluster containing the progenitor of this SNR blew a large stellar wind bubble, into which shocks are now propagating. A shell of molecular gas containing protostar candidates was found to be surrounding the SNR (Junkes et al. 1992). Figure 12 shows two regions in which infrared filaments follow the radio shell. The features are located along the nonthermal, western hemisphere of the radio shell evident at low frequencies (Velusamy et al. 1986). These are likely the locations of shocks into the wind-blown bubble and/or molecular cloud. The western filament is centered on $\alpha = 19^{\rm h}32^{\rm m}07\overset{\rm s}{.}7$, $\delta = +19^\circ02'56''$, and the northern filament is centered on $\alpha = 19^{\rm h}33^{\rm m}12\overset{\rm s}{.}6$, $\delta = +19^\circ16'20''$. The colors of the filaments are similar to photodissociation regions, so it is not certain whether the emission is due to shocks. However, there is an infrared shell

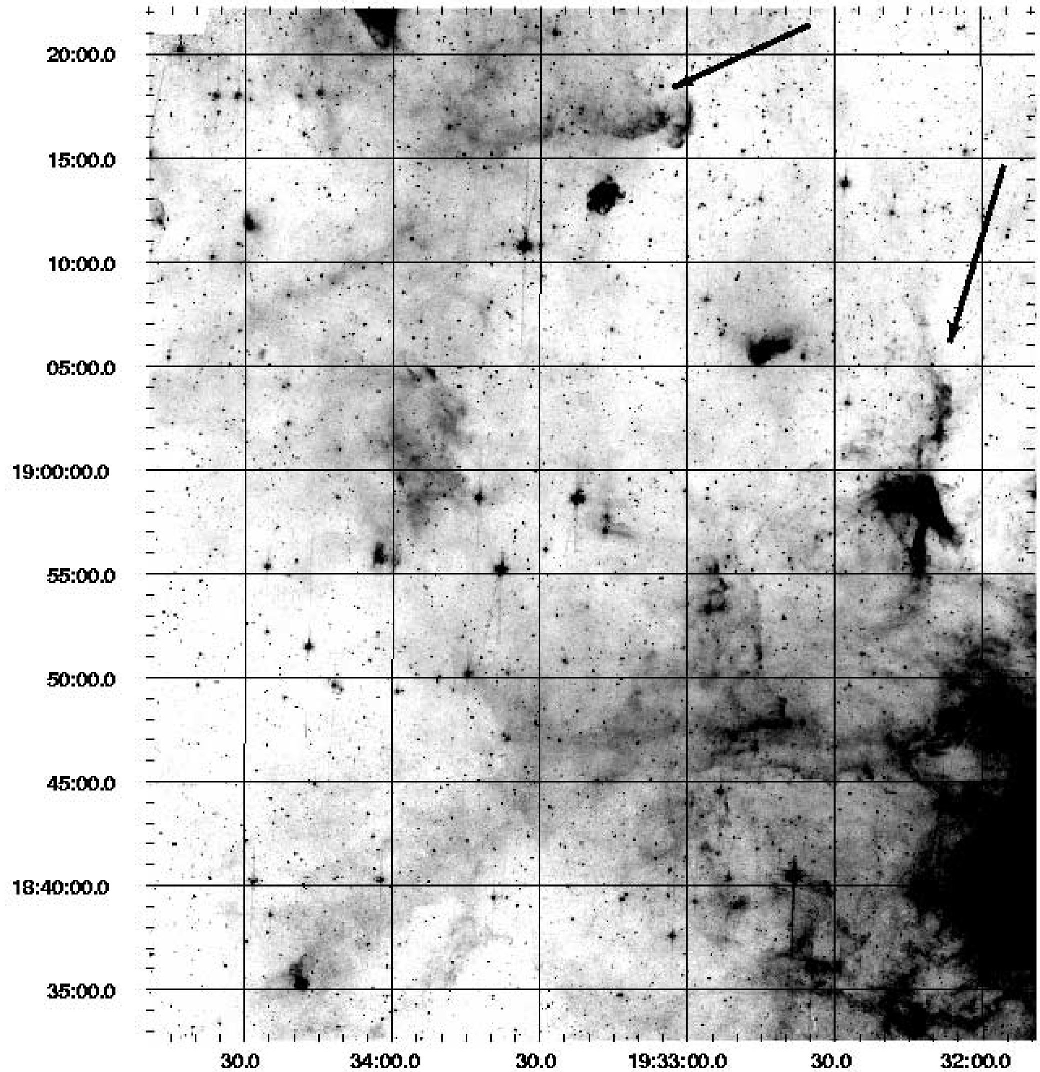

FIG. 12.—*Spitzer* IRAC 8 μm image of the SNR G54.4−0.3. The two filaments discussed in the text are marked with arrows.

in both the 5.8 and 8 μm images, approximately following much of the radio shell. Bright H II regions are located within the shell, with some of them (e.g., G54.38−0.05) possibly connecting with shell filaments. These could be a generation of stars that has formed in the shell surrounding the progenitor of the SNR (Junkes et al. 1992).

G55.0+0.3.—A large diffuse arc (3′ wide) possibly relates to the eastern radio shell, but the association is not clear.

Kes 17 (G304.6+0.1): Kes 17 is a relatively unstudied SNR. The *Spitzer* IRAC images reveal bright mid-infrared emission shown in Figure 13. The images show bright channel 2 emission (Fig. 13, *green*; likely due to shocked H_2) in the northwestern rim. Detailed arc structures are noticeable in the images, and the remnant is bright in all IRAC channels. The IRAC colors of the pair of thin isolated filaments near $\alpha = 13^h05^m46\overset{s}{.}2$, $\delta = -62°38'33''$ are somewhat more extreme (brighter in channels 1 and 3, relative to channel 4) than those toward the brightest part of shell (see Table 2). Based on the colors and the detailed morphological agreement of the images in all four channels—channel 1 in particular is not expected from ionic shocks—most of the mid-infrared emission from the shell could be from molecular shocks. The radio continuum emission shows clear shells in the northwest and south. Infrared dark clouds and globules are present north of Kes 17 ($\alpha = 13^h06^m33\overset{s}{.}5$, $\delta = -62°34'00\overset{''}{.}3$), which includes green sources (possible protostars) and possible compact H II regions. It is not known whether this star-forming region is associated with (or even at the same distance as) Kes 17.

G308.8−0.1.—This large remnant comprises a very bright northern bar (G308.7+0.0) with a southward projection, and a southern arc (G308.9−0.2). Interpreted as a single SNR, this remnant's diameter is 25′, it contains the pulsar J1341−6220, and it is located at ~7 kpc, behind most of the bright H II regions in the field (Caswell et al. 1992). The IRAC images contain a wealth of emission; the brightest emission is obviously associated with the brightest H II regions. Two features are of interest with regard to the SNR. First, following the entire extent of the northern bar there is a dark cloud. In fact, the northern bar seems to nestle within a void of infrared emission. Within the dark cloud there are three embedded sources: $\alpha = 13^h40^m20\overset{s}{.}7$, $\delta = -62°16'34''$ (very red point source, probable massive protostar), $\alpha = 13^h40^m57\overset{s}{.}0$, $\delta = -62°13'05''$, and $\alpha = 13^h32^m03\overset{s}{.}0$, $\delta = -62°11'41''$ (two bright red blobs probably containing young

Fig. 13.—*Spitzer* IRAC color image of the SNR Kes 17. The image is in equatorial coordinates and has size $13' \times 11'$.

B stars). It is hard to say whether or how this dark cloud and its embedded sources are related to the remnant, particularly if the remnant is relatively distant. The second relevant infrared feature is extensive filamentary emission within the southern arc (G308.9−0.2). A remarkable set of bright filaments is near $\alpha = 13^{\rm h}42^{\rm m}08\overset{\rm s}{.}5$, $\delta = -62°32'45''$; the IRAC colors of these filaments are 0.02/0.02/0.36/1, similar to normal, unshocked interstellar PAHs. The 5.8 μm image seems to form a shell including the southern arc, with a northern boundary far to the south of G308.7+0.0. Based only on the radio and infrared emission, we might conclude that there are two separate remnants. However, any infrared emission from the northern portion of the SNR is actually extinguished by the dark cloud that is seen in projection against G308.7+0.0 (regardless whether the dark cloud and G308.7+0.0 are associated).

Kes 20B (G310.6−0.3).—Very dark clouds surround this remnant, including remarkable large clouds completely opaque at 8 μm to the north and east. While the present data do not clearly reveal an interaction with these clouds, an interaction may be occurring to the north, where the radio contours run along the long axis of a dark cloud. Some 8 μm emission appears around the border of the remnant but does not have a detailed relationship to the radio contours and could be unrelated. A notable feature occurs inside the remnant, approximately along a faint inner radio ridge. It is a thin filament, centered on $\alpha = 13^{\rm h}58^{\rm m}08^{\rm s}$, $\delta = -62°07'03''$, with position angle 67° east of north and length 23″, and it has IRAC colors consistent with a molecular shock. Without a higher resolution radio image (to correlate with the infrared filament) or a more sensitive infrared image (to find other such features) it is not possible to tell whether this is a shock front into a molecular cloud or a massive molecular outflow from a young stellar object. There is no obvious young stellar object in the IRAC images. Based on the present data we can only suggest that some infrared emission *may* be related to the remnant, but there is not enough evidence to call this remnant a detection.

Kes 20A (G310.8−0.4): This large remnant (Fig. 14) has a distinctive radio morphology defined by a very bright ridge running roughly north-south, defining what could be the eastern hemisphere of a shell; the western hemisphere is not clear in the nonthermal radio image. Extensive infrared emission approximately follows the radio ridge. The infrared emission breaks into many narrow clumps and arcs. Based on the infrared image alone, these would appear to be small H II regions or reflection nebulae. Indeed, numerous similar features that exist throughout the region are clearly unrelated to Kes 20A. The brightest such H II regions are evident in the MOST radio image as individual sources, clearly distinct from the nonthermal ridge that defines the remnant. In addition to the emission along the eastern ridge, similar filamentary infrared emission occupies part of what would be the interior of the remnant based on the incomplete-shell radio morphology. Additional, similar infrared emission is located outside the remnant and is clearly not directly related. The high density of H II regions and proximity to the SNR Kes 20B show this region to be rife with massive stars. Thus, the emission that appears plausibly associated with Kes 20A could be a chance association or a second-generation association due to younger stars that formed in

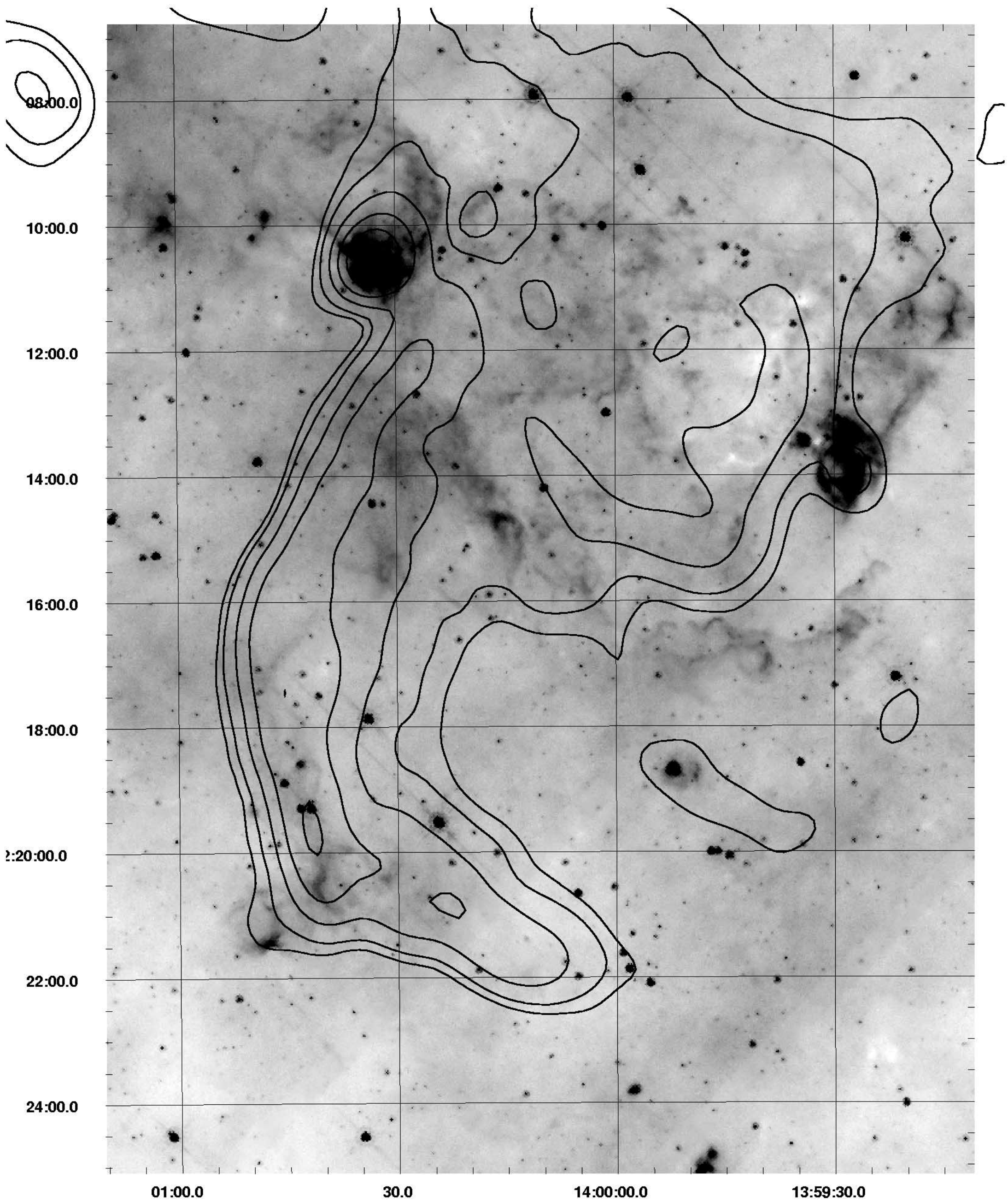

FIG. 14.—*Spitzer* IRAC image of the SNR Kes 20A, with radio continuum contours from the MSC overlaid.

a wind-blown bubble generated by the progenitor. A slice through the southeastern portion of the remnant yields infrared colors 0.13/0.13/0.67/1 that do not match the color templates described above very well but are generally similar to those of photodissociation regions, which supports a second-generation (as opposed to shock-powered) origin for the present infrared emission.

G311.5−0.3: This shell-type remnant is one of the most easily detected in the present survey because it so clearly follows the entire radio shell and is in a relatively uncluttered region. Cohen & Green (2001) compared MOST observations with 8.3 μm observations made with the *Midcourse Space Experiment* (*MSX*) and reported no detection. Figure 15 shows the *Spitzer* IRAC image, which is significantly deeper than *MSX*, so the SNR is evident in all four channels. The IRAC images show a nearly complete shell of infrared emission, corresponding well with the radio shell. Bright narrow filaments line the western edge of the SNR, with two bright ridges giving a "braided" appearance over a significant portion of the western shell. The infrared shell is particular bright near $\alpha = 14^{\mathrm{h}}05^{\mathrm{m}}21\overset{\mathrm{s}}{.}9$, $\delta = -61°58'06''$, and a less-confused filament nearby ($\alpha = 14^{\mathrm{h}}05^{\mathrm{m}}22\overset{\mathrm{s}}{.}6$, $\delta = -61°57'22''$) has IRAC color ratios 0.3/0.4/1/1, suggesting that the IRAC emission is from shocked gas. Two bright, red, compact sources at $\alpha = 14^{\mathrm{h}}05^{\mathrm{m}}24\overset{\mathrm{s}}{.}3$, $\delta = -61°57'07''$ and $\alpha = 14^{\mathrm{h}}05^{\mathrm{m}}23\overset{\mathrm{s}}{.}5$, $\delta = -61°56'58''$ are possibly Class 0 protostars located just at the edge of the SNR.

Kes 27 (G327.4+0.4): The mid-infrared image shows a set of bright filaments with diffuse emission centered on a radio peak within the remnant near J154912−534420 (G327.39+0.47). Figure 16 shows the correspondence between this region and the radio shell. This filamentary source could be the location of

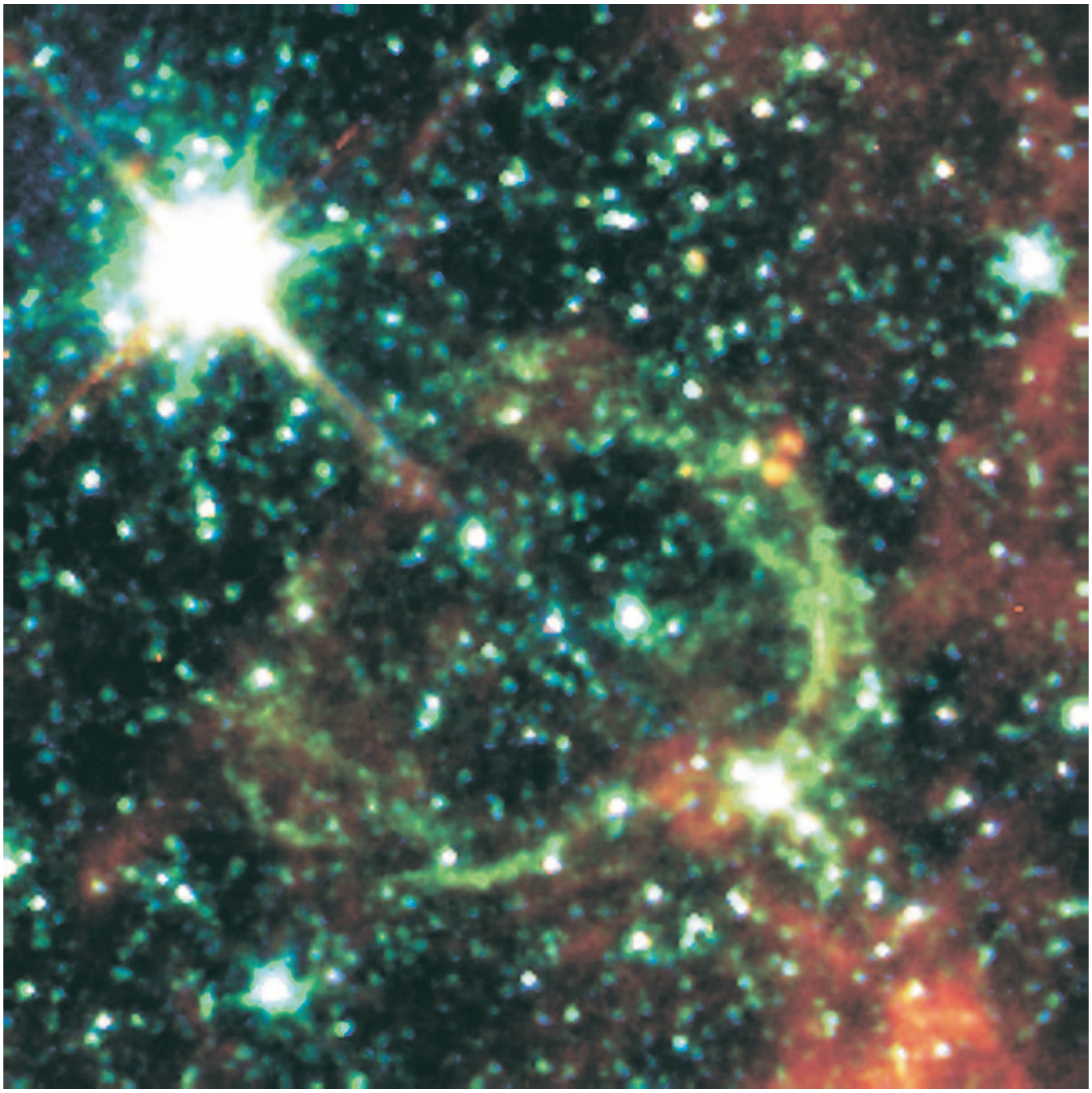

FIG. 15.—*Spitzer* IRAC color image of the SNR G311.5−0.3, with red = 8 μm, green = 4.5 μm, blue = 3.6 μm, and magenta = 5.8 μm minus a scaled 8 μm image. The entire shell of the SNR is evident, with a double-stranded morphology.

shocks into a dense cloud, possibly containing an embedded massive star, so we consider it in more detail. The MOST 843 MHz image (Whiteoak & Green 1996) shows a resolved but simple (centrally condensed) peak with a FWHM of $2\farcm2$ and a flux of approximately 0.4 Jy (from aperture photometry centered on the source with annular background removal). The Parkes 5 GHz image (Milne & Dickel 1975) does not show a corresponding structure, at least partially due to its low angular resolution ($4\farcm4$). If the source is an H II region with thermal spectrum, the flux at 5 GHz would be $\sim$0.2 Jy and the brightness temperature would be $\sim$0.3 K after diluting to the Parkes 5 GHz beam. On the other hand, if the source is nonthermal with spectral index 0.7, then the brightness temperature at 5 GHz would be 0.06 K. There is no structure in the 5 GHz image above 0.2 K, which is consistent with nonthermal emission and marginally inconsistent with thermal emission. McClure-Griffiths et al. (2001) show a 1420 MHz continuum image of the remnant (their Fig. 13). The radio peak corresponding to the infrared region is evident in their image, with a flux of approximately 0.2 Jy (counting contours). The 1420 and 843 MHz contour maps are nearly identical after a linear transformation, indicating that the infrared filamentary source has about the same spectral index as the rest of the remnant emission. Improved radio continuum observations are needed to assess the nature of the source. The mid-infrared colors of this region are more typical of PAH-dominated photodissociation regions than shocked gas. McClure-Griffiths et al. (2001) show from 21 cm line observations that there is an H I ridge just outside the southwestern radio contours. There are no obvious protostar candidates in the region, so the impact has evidently not triggered star formation; this is not surprising given that the remnant is thought to be relatively young, with estimates of 2400 yr (McClure-Griffiths et al. 2001) and 3500 yr (Seward et al. 1996) (cf. $>8\times10^4$ yr from Enoguchi et al. [2002]). The true nature of this region awaits future investigation.

G329.7+0.4.—The southwestern corner of this remnant has bright, extended mid-infrared emission that follows some of the radio structures, in particular the southwestern corner of the remnant and a bright spur penetrating into the remnant from $\alpha = 16^{\rm h}00^{\rm m}39\fs9$, $\delta = -52\arcdeg30'46''$ to $\alpha = 16^{\rm h}01^{\rm m}10\fs3$, $\delta = -52\arcdeg25'24''$ (and beyond). The corner and spur have similar brightness to some H II regions, but their orientation along a radio filament that appears to be part of the remnant makes them plausibly part of the remnant. On the other hand, there are some mid-infrared spurs that appear related to this same region but

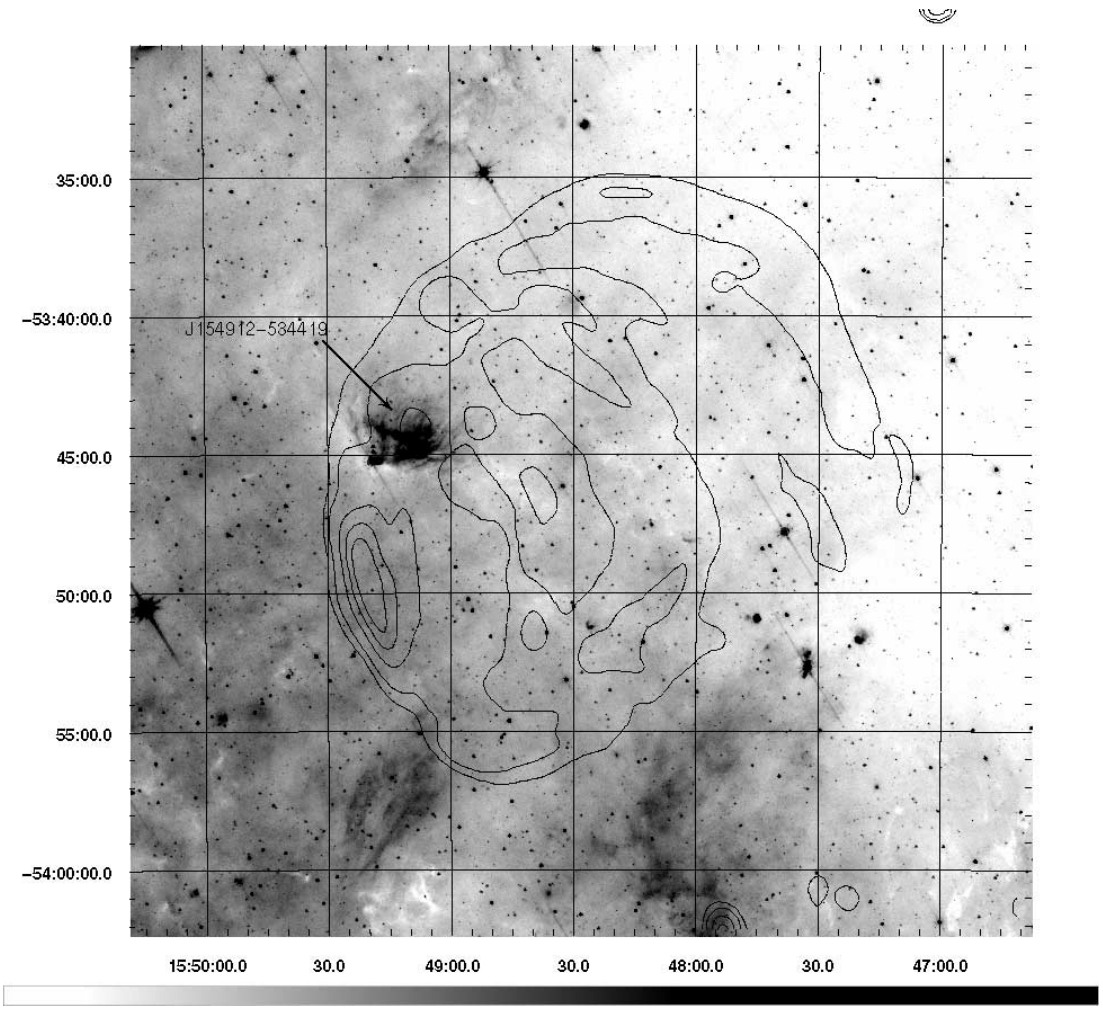

FIG. 16.—*Spitzer* IRAC 8 μm image of the SNR Kes 27, with radio contours from the NVSS overlaid. [*See the electronic edition of the Journal for a color version of this figure*.]

directed well outside the remnant. The colors of the bright bar are 0.03/0.02/0.33/1 (toward a location at which the 8 μm surface brightness is 66 MJy sr^{-1}) look like PAH emission or an H II region. A "shell" of mid-infrared emission surrounds the remnant on the eastern and southern sides, connecting to the bright southwestern corner and the western side of the remnant. This "shell" breaks into some moderately bright patches that may be individual H II regions or photodissociation regions from B stars. The overall boxlike shape of the region is very similar to the outer boundary of the nonthermal emission from the SNR. Therefore, we suspect that it is in fact related to the remnant, even though it is unlikely to be emission from shocked dust and gas. Instead, it probably represents a fossil shell, due to the stellar winds and supernovae of the previous generation of massive stars, into which the present remnant is now expanding. A relatively diffuse part of the shell has colors 0.05/0.04/0.6/1 (toward a location at which the 8 μm surface brightness is 11 MJy sr^{-1}), most similar to PAH regions or H II regions.

RCW 103 (G332.4−0.4): The IRAC images (Fig. 17) in all four channels show relatively bright, diffuse emission associated with the SNR RCW 103. In particular, channel 2 shows strong emission at the southern shell and faint emission in the northwestern and western shell. H_2, [Fe II], and [Ar II] lines were previously detected in *ISO* spectra, and the emission was spatially resolved in the ISOCAM field-of-view 1$'$.5 image (Oliva et al. 1999). Therefore, we measure the IRAC color from two positions of the SNR. A slice through the filament near $\alpha = 16^{\rm h}17^{\rm m}32^{\rm s}.8$, $\delta = -51°06'28''$ yields colors 0.14/0.28/0.86/1 (with 8 μm brightness 14.5 MJy sr^{-1}), most likely dominated by shocked molecules (but with some ionic contribution in channel 3). Much of the southern rim has such colors. A thin filament near $\alpha = 16^{\rm h}17^{\rm m}45^{\rm s}.7$, $\delta = -51°04'58''$ (Table 2) is undetected in channel 1 despite being very distinct in channel 3 indicating ionic shocks. The two types of emitting regions can be discerned in Figure 17, with the primarily molecular shocks appearing green and the primarily ionic shocks appearing magenta. There are a number of H II regions and dark clouds surrounding RCW 103.

Kes 32 (G332.4+0.1).—There is no mid-infrared emission corresponding to the radio contours from MOST. However, there is a very bright infrared H II region in the southwestern part of the remnant. The H II region is centered near $\alpha = 16^{\rm h}15^{\rm m}37^{\rm s}.9$, $\delta = -50°44'06''$ and has a central cavity containing what appears to be a cluster of young stars. Protrusions extend from this H II region in many directions, including narrow filaments and what appears to be a very large "plume" extending to the northwest of the H II region, directly across the western half of Kes 32. It is not clear which features are associated with the remnant and which are associated with the H II region. However, the high-resolution *Spitzer* IRAC image shows the plume connects directly to the H II region and is most likely associated with it. This contradicts an earlier conjecture that the plume, which can been seen in radio images, could be a jet of energetic particles from the

FIG. 17.—*Spitzer* IRAC color image of the SNR RCW 103, with red = 8 μm, green = 4.5 μm, blue = 3.6 μm, and magenta = 5.8 μm minus a scaled 8 μm image. The SNR is most clearly separated from the diffuse Galactic emission by its 4.5 μm emission, but it is detected in all four IRAC channels. There are at least two distinct emitting regions; the dominant one (seen in all four channels) is green in this rendition, while a fainter one (most noticeable at 5.8 μm) is magenta.

stellar remnant of Kes 32 (Roger et al. 1985). Instead, we suspect that the plume originates from the H II region and is being ionized by the current generation of young stars within it.

G344.7−0.1: G344.7−0.1 has not been well studied, but the radio morphology is shell-like with a bright northwestern shell (Dubner et al. 1993). Figure 18 reveals an area of irregularly structured infrared emission about 2′ in diameter near $\alpha = 17^{\rm h}03^{\rm m}55\overset{\rm s}{.}1$, $\delta = -41°40'43''$. The colors (Table 2) suggest that the emission is likely due to shocked ionized gas. Figure 18 shows the mid-infrared emission coinciding with the central radio peak from the MSC (Whiteoak & Green 1996). This is the first detection in the infrared; it was not seen in previous *IRAS* surveys (Arendt 1989; Saken et al. 1992).

G346.6−0.2: The SNR is surrounded in the north and west by diffuse infrared emission (5.8–8 μm). The emission associated with the remnant is a narrow rim that follows the southern radio shell. The IRAC colors of the rim are very distinct, so the rim is evident in the color image (Fig. 19, *left*). This southern rim more or less connects the three OH 1720 MHz masers associated with the remnant. The IRAC colors suggest molecular shocks, consistent with their close association with the OH masers. In addition to the southern rim, there is possibly some infrared emission following the northern shell, but it is not readily evident in the figures.

CTB 37A (G348.5+0.1): Figure 20 (*top*) shows patches and filaments of 4.5 μm (*green*) emission indicating shocked H_2 in the north, as well as patches and filaments of 5.8–8 μm (*red*) emission in the center and east of CTB 37A. The radio image has a "breakout" morphology suggesting impact into a medium denser in the northeast and less dense in the southwest. The 5.8–8 μm image (Fig. 20, *bottom*) shows that the mid-infrared emission, probably from shocked gas, has a similar morphology. Green patches in the north correspond to the northernmost of the eight OH 1720 MHz masers with velocities around -65 km s^{-1}, which are associated with CTB 37A. None of the other maser spots in this remnant have associated 4.5 μm spots, although some faint, patchy emission is in the vicinity of most of the masers associated with CTB 37A.

The patch of green mid-infrared emission in the northeast is almost certainly shocked H_2 gas; the colors in IRAC channels (Table 2) are similar to that expected for H_2 + CO and not consistent with PAH emission. The red filaments in the IRAC image are clearly different, both in morphology and color. The arc near $\alpha = 17^{\rm h}14^{\rm m}14\overset{\rm s}{.}7$, $\delta = -38°31'13''$ has IRAC colors 0.07/0.04/0.42/1, consistent with PAH emission. Since there are so many regions with similar colors, it is possible that some of these red filaments are unrelated to the remnant. We suspect, however, that many of the infrared structures within the radio remnant are in fact related to the remnant. For example, the relatively bright, semicircular region including the filament mentioned above and the bright patch and associated filaments centered around $\alpha = 17^{\rm h}14^{\rm m}22\overset{\rm s}{.}6$, $\delta = -38°35'06''$ are all located at the transition between the bright radio half-shell and the fainter extended emission that appears to be the opening of the blowout, probably near

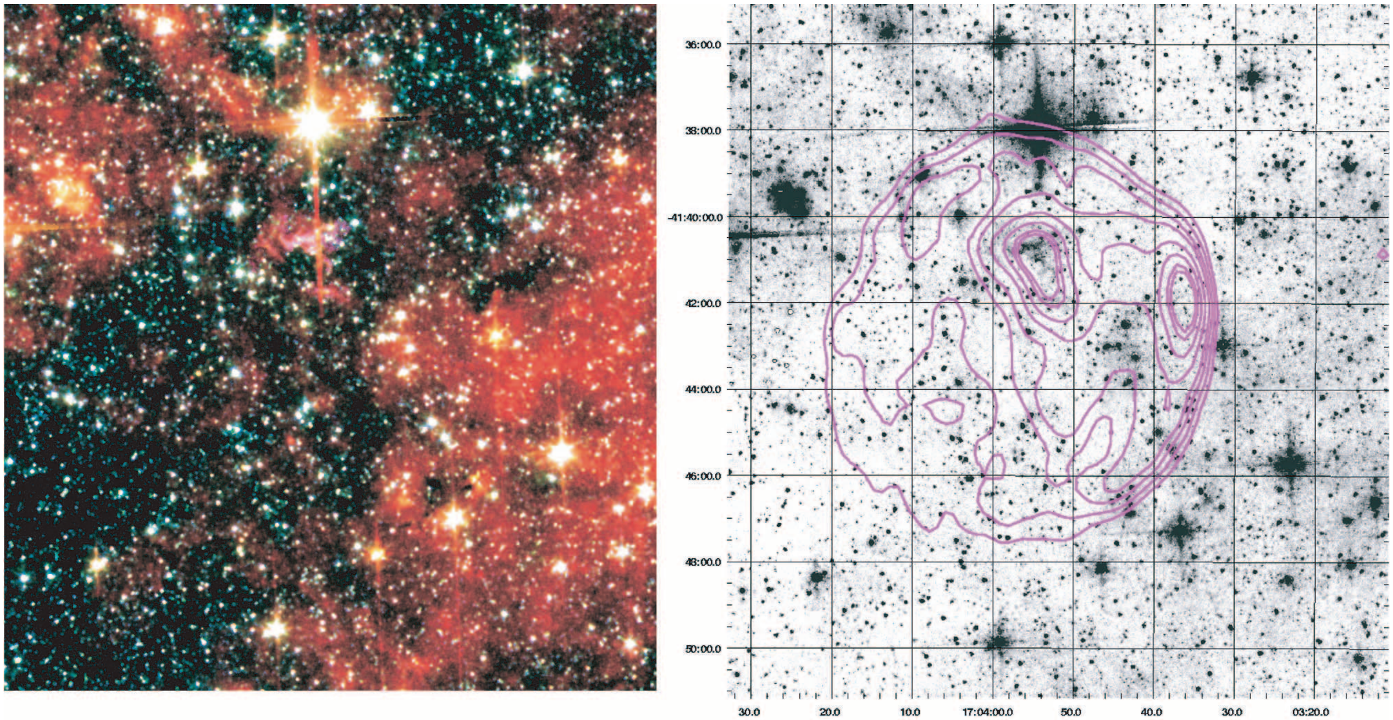

FIG. 18.—*Left*: *Spitzer* IRAC color image of G344.7−0.1, with red = channel 4, orange = channel 3, green = channel 2, blue = channel 1, and magenta = channel 3 − (0.3 × channel 4). The filament associated with the northern radio peak in the SNR is relatively bright in channel 3 and appears "magenta" in this image. *Right*: *Spitzer* IRAC channel 3 image of G344.7−0.1, with radio contours from the MSC overlaid. The gray scale ranges from 15 to 30 MJy sr^{-1}. The northern, interior radio peak has an apparently associated mid-infrared filament.

the surface of the preexplosion cloud. Long filaments, especially visible in the 5.8–8 μm images, extend along the fainter northwestern and southwestern portions of the fainter, extended radio emission in the "blowout" shell, accurately delineating the boundary. The colors of these extended filaments are consistent with PAH emission.

G348.5−0.0: This remnant is partially superposed on CTB 37A; high-resolution radio observations showed that G348.5−0.0 is a separate remnant (Kassim et al. 1991). The *Spitzer* IRAC image shows a narrow arc of emission that closely follows the radio rim. The correspondence between the 5.8 μm filament detected by IRAC (Fig. 20, *bottom*) and the 6 cm radio rim detected with the VLA (Fig. 6 of Kassim et al. 1991) is precise, so the association of these features is beyond doubt. The filament is narrow—unresolved ($<3''$) to IRAC. The filament is detected IRAC channels 2–4, with color ratios (Table 2) measured toward $\alpha = 17^{\rm h}15^{\rm m}04\overset{\rm s}{.}6$, $\delta = -38°33'40''$. The 5.8/8 μm ratio is much too high to be PAH emission, and the filament is

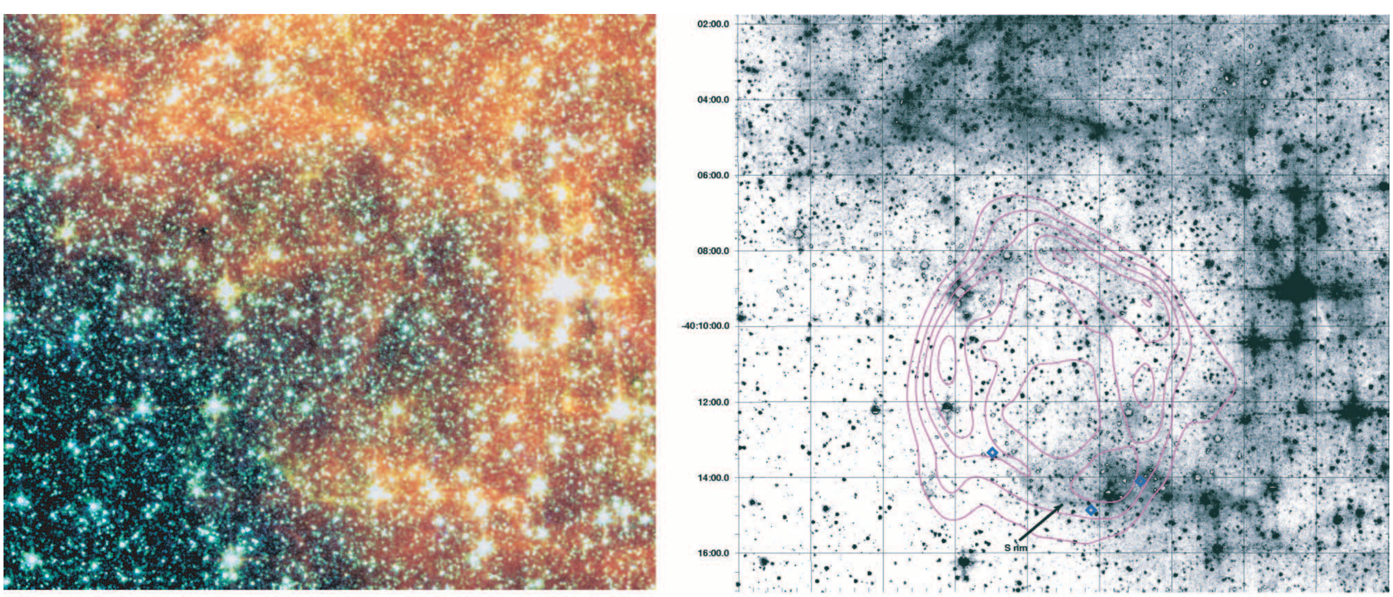

FIG. 19.—*Left*: *Spitzer* IRAC color image of G346.6−0.2, with red = 8 μm, green = 4.5 μm, and blue = 3.6 μm. Radio contours from the MSC are overlaid in magenta; contour levels are 50, 100, 150, 200, and 250 mJy beam^{-1} in a $43'' \times 67''$ beam. *Right*: *Spitzer* IRAC 5.8 μm image of G346.6−0.2 with radio contours (*magenta*) and the locations of OH 1720 MHz masers (*blue diamonds*) superposed. The gray scale ranges from 8 to 43 MJy sr^{-1}.

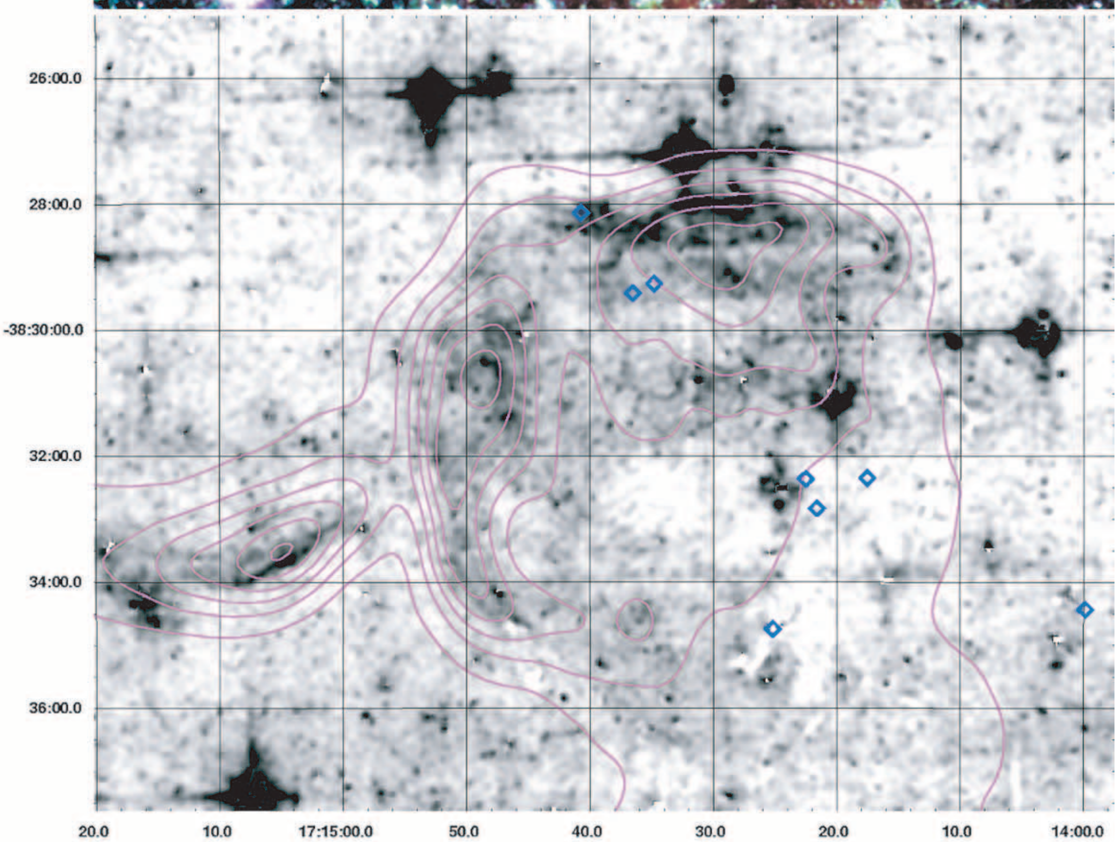

FIG. 20.— *Top*: *Spitzer* IRAC (5.8 μm) $-$ [0.361(8 μm)] image of the SNRs CTB 37A (G348.5+0.1) and G348.5$-$0.0. OH 1720 MHz maser positions (Frail et al. 1996) are overlaid as diamonds. No radio contours are overlaid to avoid confusing the image, in which diffuse emission is evident from both SNRs. The SNR CTB 37A is evident as a hemispheric shell including the relatively bright northern arcs at $\alpha = 17^{\rm h}14^{\rm m}35^{\rm s}$, $\delta = -38°29'30''$ and the western shell extending through $\alpha = 17^{\rm h}14^{\rm m}51^{\rm s}$, $\delta = -38°31'50''$. The SNR G345.8$-$0.0 is evident as a short arc (labeled) passing through $\alpha = 17^{\rm h}15^{\rm m}05^{\rm s}$, $\delta = -38°33'43''$. *Bottom*: *Spitzer* IRAC color image of the SNRs CTB 37A (G348.5+0.1) and G348.5$-$0.0, with red = 8 μm, green = 4.5 μm, blue = 3.6 μm, and magenta = (5.8 μm) $-$ [0.361(8 μm)]. The patch of green infrared emission in the northeast is most likely shocked molecular gas where the blast wave is impacting very dense gas. This green patch contains the northernmost OH 1720 MHz maser, which is at -64.3 km s^{-1} (Frail et al. 1996), like most of the other masers that are associated with CTB 37A. The SNR G348.5$-$0.0 appears as a thin magenta filament (see Fig. 20 for a guide), suggesting ionic shocks. The western shell of CTB 37A is not as easy to see in this multiwavelength image but has a magenta tint, also suggesting ionic shocks.

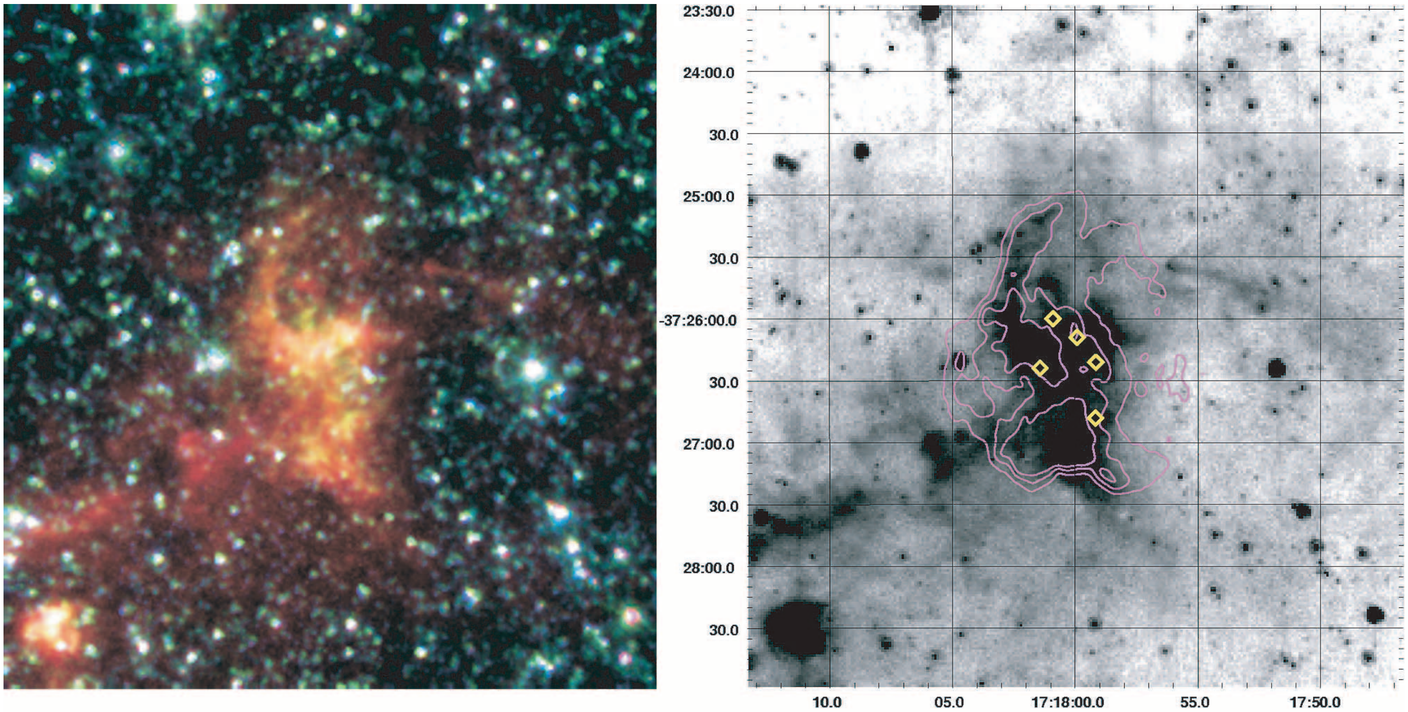

Fig. 21.—*Spitzer* IRAC color image (*left*) and 5.8 μm image (*right*) of the SNR G349.7+0.2. For the color image, red = 8 μm, green = 4.5 μm, blue = 3.6 μm, and magenta = (5.8 μm) − [0.361(8 μm)]. Radio 20 cm contours are overlaid on the channel 3 image.

most likely dominated by emission lines from shocked gas. The radio extent of this remnant can be seen in sensitive VLA images (Kassim et al. 1991) to extend across the northwestern part of CTB 37A and emerge from its northern rim. The second and third northernmost OH 1720 MHz masers in this region are at $V_{\rm LSR} = -23$ and -21 km s^{-1}, clearly distinct from the velocities of the other eight masers that are associated with CTB 37A. There are also distinct molecular clouds at these velocities that are likely related to the remnants, with the -23 km s^{-1} cloud situated just west of G348.5−0.0 having the masers at its edge; this cloud is most likely associated with G348.5−0.0 (Reynoso & Mangum 2000). The *Spitzer* IRAC images further support the idea that G348.5−0.0 is interacting with a dense cloud, because the infrared emission most likely traces relatively dense, shocked gas. The patch of green infrared emission in the northern part of CTB 37A is in the region in which that remnant overlaps with G348.5−0.0 and could contain contributions from both remnants, but we associate it with CTB 37A based on the morphology (infrared filaments follow the CTB 37A radio shape, not G348.5−0.0, in this patch) and associated maser velocities. There is no infrared emission that appears related to the two OH masers associated with G348.5−0.0. The infrared filament along the radio rim of G348.5−0.0 is, however, clearly part of this remnant, and projecting it to the west, taking into account the curvature of the radio shell, it passes through the OH masers at -23 and -21 km s^{-1}. This remnant and CTB 37A are a special case of two different remnants interacting with two different molecular clouds, all superposed in the same several arcminutes of the sky.

G349.7+0.2: This is one of the brightest SNRs in the survey, and owing to its great distance it is the most luminous. Its X-ray brightness makes it one of the most luminous X-ray remnants, and it may be younger than 3000 yr (Slane et al. 2002). The radio image was constructed by combining VLA data in A, C, CD, and D configurations, with $5''.0 \times 2''.1$ resolution (Brogan et al. 2000). This remnant was shown to be interacting with a large molecular shell by Reynoso & Mangum (2001), and OH maser emission was detected by Frail et al. (1996). The mid-infrared emission is detected in all IRAC bands (Fig. 21); it is very bright at 5.8 μm and easily discerned at 4.5 and 8 μm. There are 4.5 and 5.8 μm emission peaks near four of the five OH 1720 MHz maser spots (all except the first from Frail et al. [1996]); these peaks are not as prominent at 8 μm. Shocked H_2 line emission is a likely contributor to the 4.5 and 5.8 μm wave bands. The 8 μm image may contain an emission mechanism in addition to the $H_2 S(5)$ line, such as [Ar II] 6.99 μm. There is a filament of red (mostly 8 μm) emission extending from the SNR toward the west; it extends beyond the boundary of Figure 21 and has colors similar to other extended emission in the field nearby. This is apparently part of the dense cloud with which the SNR is interacting. The unusual morphology of the remnant, with its shell much brighter on the western side, is caused by the shock propagating into the long axis of a roughly cylindrical cloud.

5. CONCLUSIONS

The colors of the detected SNRs reveal a wide range of emission mechanisms. Figure 22 shows the observed colors for 1–2 spots per remnant together with bounding regions for molecular shocks, ionic shocks, and PAH emission from Figure 2. Nine spots have colors consistent with molecular shocks, three have colors consistent with ionic shocks, and four are consistent with PAH emission from unshocked ISM. Of the remaining, all but one are intermediate between molecular and ionic shocks and probably represent a mixture of shock types. One spot, the Kes 69 ridge, falls sufficiently outside the bounds of emission mechanisms considered here that its colors cannot be explained by the mechanisms discussed here.

The SNRs with colors suggesting molecular shocks include 3C 391, Kes 17, G346.6−0.2, G311.5−0.3, G344.7−0.1, Kes 20, and G11.2−0.3. Two of these (3C 391 and G346.2−0.2) have associated OH 1720 MHz masers (Frail et al. 1996; Green et al. 1997). For comparison, only 14% of the entire sample of 95 remnants have OH 1720 MHz masers, so the association of

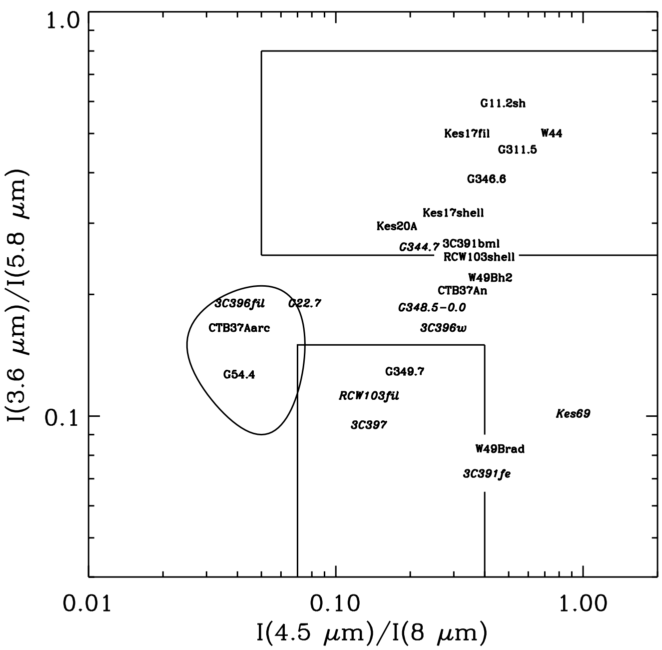

Fig. 22.—IRAC color-color diagram for one or two locations in each of the detected SNRs from this survey. The predicted colors of molecular shocks (*upper rectangle*), ionic shocks (*lower rectangle*), and PAHs (*ellipse*) are copied from Fig. 2 to aid interpretation. Labels in italics are for remnants with upper limits (generally, these are nondetections in channel 1, so the actual color would be downward from the label in this figure).

these infrared colors with molecular shocks is not a chance coincidence. A total of 7 out of 18 IRAC-detected remnants have associated masers; the 39% association rate is again clearly not by chance. The remnants with colors suggesting molecular shocks but lacking OH masers may not have the specific, narrow physical conditions required to generate the maser inversions. For example, 3C 391 has a strong interaction with a giant molecular cloud on its bright radio northwestern ridge, but the OH masers are only present in two spots to the edge of the main interaction (Reach et al. 2002).

One of the remnants with IRAC colors in the "molecular" region of the color-color diagram is the historical SNR G11.2−0.3. As discussed above, the mid-infrared emission from this young SNR may not be exclusively from molecular lines. Dust continuum is also unlikely to be the source of the unusual colors, because it would make the 8 μm band bright and move the colors to the left. Synchrotron radiation could contribute an extra source of 3.6 and 4.5 μm emission and could possibly explain the colors. Otherwise, the colors could indicate unusual abundances; further spectroscopic observations are needed to understand this SNR.

The SNRs with colors suggesting ionic shocks are 3C 397, W49B, and 3C 391 (northwestern ridge). The radio emission from all three is bright and highly structured, with bright near-infrared [Fe II] that correlates in detail with the radio structure.

The remnants with colors suggesting a mixture of molecular and ionic shocks are RCW 103, CTB 37A, G348.5−0.0, and 3C 396. In RCW 103, spectroscopy clearly reveals bright lines from both molecular and ionic shocks (Oliva et al. 1999). For CTB 37A and G348.5−0.0, OH 1720 MHz masers are associated, suggesting likely shocked molecular gas. The presence of both types of shock in an SNR is not unexpected, as the shocked dense clumps that cool via molecular lines are likely immersed in a lower density medium that, when shocked, cools via ionic lines. This is clearly seen in the *ISO* spectra of W28, 3C 391, W44, IC 443, and RCW 103 (Reach & Rho 2000; Oliva et al. 1999).

The details of the emission mechanism for each SNR remain to be determined with follow-up spectroscopy and comparison to ground-based observations. However, the IRAC survey already suggests a trend such that mid-infrared-detected SNRs tend to have colors suggesting shocks into dense gas. While this is an obvious selection effect, because many important cooling lines of such shocks are present in the mid-infrared the sheer number of such detections suggests that molecular cloud interactions are not uncommon: at least 6% of SNRs in our survey show infrared colors suggesting molecular shocks. Some of these SNRs suspected to be interacting with molecular clouds have been studied relatively little and await further investigation.

This work is based in part on observations made with the *Spitzer Space Telescope*, which is operated by the Jet Propulsion Laboratory, California Institute of Technology, under NASA contract 1407. We thank Rick Arendt for his helpful comments.

REFERENCES

Arendt, R. G. 1989, ApJS, 70, 181
Arendt, R. G., Dwek, E., & Moseley, S. H. 1999, ApJ, 521, 234
Benjamin, R. A., et al. 2003, PASP, 115, 953
Brogan, C. L., Frail, D. A., Goss, W. M., & Troland, T. H. 2000, ApJ, 537, 875
Brogan, C. L., Lazio, T. J., Kassim, N. E., & Dyer, K. K. 2005, AJ, 130, 148
Caswell, J. L., Kesteven, M. J., Stewart, R. T., Milne, D. K., & Haynes, R. F. 1992, ApJ, 399, L151
Cohen, M., & Green, A. J. 2001, MNRAS, 325, 531
Condon, J. J., Cotton, W. D., Greisen, E. W., Yin, Q. F., Perley, R. A., Taylor, G. B., & Broderick, J. J. 1998, AJ, 115, 1693 (NVSS)
Draine, B. T., & Lee, H. M. 1984, ApJ, 285, 89
Dubner, G. M., Moffett, D. A., Goss, W. M., & Winkler, P. F. 1993, AJ, 105, 2251
Enoguchi, H., Tsunemi, H., Miyata, E., & Yoshita, K. 2002, PASJ, 54, 229
Fazio, G. G., et al. 2004, ApJS, 154, 10
Fixsen, D. J., Moseley, S. H., & Arendt, R. G. 2000, ApJS, 128, 651
Frail, D. A., Goss, W. M., Reynoso, E. M., Giacani, E. B., Green, A. J., & Otrupcek, R. 1996, AJ, 111, 1651
Green, A. J., Frail, D. A., Goss, W. M., & Otrupcek, R. 1997, AJ, 114, 2058
Green, D. A. 2004, Bull. Astron. Soc. India, 32, 335
Green, D. A., & Dewdney, P. E. 1992, MNRAS, 254, 686
Hwang, U., Petre, R., & Hughes, J. P. 2000, ApJ, 532, 970
Jones, A. P., Tielens, A. G. G. M., & Hollenbach, D. J. 1996, ApJ, 469, 740
Junkes, N., Fürst, E., & Reich, W. 1992, A&A, 261, 289
Kaspi, V. M., Roberts, M. E., Vasisht, G., Gotthelf, E. V., Pivovaroff, M., & Kawai, N. 2001, ApJ, 560, 371
Kassim, N. E. 1992, AJ, 103, 943
Kassim, N. E., Baum, S. A., & Weiler, K. W. 1991, ApJ, 374, 212
Keohane, J., Reach, W. T., & Rho, J. 2005, ApJ, submitted
McClure-Griffiths, N. M., Green, A. J., Dickey, J. M., Gaensler, B. M., Haynes, R. F., & Wieringa, M. H. 2001, ApJ, 551, 394
Milne, D. K., & Dickel, J. R. 1975, Australian J. Phys., 28, 209
Moffett, D. A., & Reynolds, S. P. 1994, ApJ, 437, 705
Olbert, C. M., Keohane, J. W., Arnaud, K. A., Dyer, K. K., Reynolds, S. P., & Safi-Harb, S. 2003, ApJ, 592, L45
Oliva, E., Moorwood, A. F. M., Drapatz, S., Lutz, D., & Sturm, E. 1999, A&A, 343, 943
Osterbrock, D. E. 1989, Astrophysics of Gaseous Nebulae and Active Galactic Nuclei (Mill Valley: University Science Books)
Patnaik, A. R., Hunt, G. C., Salter, C. J., Shaver, P. A., & Velusamy, T. 1990, A&A, 232, 467
———. 1998, ApJ, 507, L93
Reach, W. T., & Rho, J.-H. 1999, ApJ, 511, 836
———. 2000, ApJ, 544, 843
Reach, W. T., Rho, J.-H., & Jarrett, T. H. 2005a, ApJ, 618, 297
Reach, W. T., Rho, J.-H., Jarrett, T. H., & Lagage, P.-O. 2002, ApJ, 564, 302

Reach, W. T., et al. 2005b, PASP, 117, 978
Reynoso, E. M., & Mangum, J. G. 2000, ApJ, 545, 874
———. 2001, AJ, 121, 347
Rho, J., Jarrett, T., Cutri, R., & Reach, W. T. 2001, ApJ, 547, 885
Rho, J.-H., & Petre, R. 1998, ApJ, 503, L167
Rho, J., Petre, R., Schlegel, E. M., & Hester, J. J. 1994, ApJ, 430, 757
Rho, J., Reynolds, S. P., Reach, W. T., Jarrett, T. H., Allen, G. E., & Wilson, J. C. 2003, ApJ, 592, 299
Roger, R. S., Milne, D. K., Kesteven, M. J., Haynes, R. F., & Wellington, K. J. 1985, Nature, 316, 44
Saken, J. M., Fesen, R. A., & Shull, J. M. 1992, ApJS, 81, 715
Seward, F. D., Kearns, K. E., & Rhode, K. L. 1996, ApJ, 471, 887
Seward, F. D., Slane, P. O., Smith, R. K., & Sun, M. 2003, ApJ, 584, 414
Slane, P., Chen, Y., Lazendic, J. S., & Hughes, J. P. 2002, ApJ, 580, 904
Tam, C., & Roberts, M. S. E. 2003, ApJ, 598, L27
Velusamy, T., Goss, W. M., & Arnal, E. M. 1986, J. Astrophys. Astron., 7, 105
Werner, M. W., et al. 2004, ApJS, 154, 1
Whiteoak, J. B. Z., & Green, A. J. 1996, A&AS, 118, 329
Yusef-Zadeh, F., Wardle, M., Rho, J., & Sakano, M. 2003, ApJ, 585, 319